

**Gorongosa by the sea: first Miocene fossil sites from the Urema Rift, central Mozambique,
and their coastal paleoenvironmental and paleoecological contexts**

Jörg M. Habermann^{a,b,c,*}, Matthias Alberti^d, Vera Aldeias^{a,e}, Zeresenay Alemseged^f, Will Archer^{e,g},
Marion Bamford^h, Dora Biroⁱ, David R. Braun^{e,j}, Cristian Capelliⁱ, Eugénia Cunha^k, Maria Ferreira da
Silva^{l,m}, Tina Lüdecke^{b,n,o}, Hilário Madiquida^p, Felipe I. Martinez^q, Jacinto Mathe^r, Enquye Negash^j, Luis
M. Paulo^s, Maria Pinto^s, Marc Stalmans^r, Frederico Tátá Regala^{a,s}, Jonathan G. Wynn^t, René Bobe^{a,b,r},
Susana Carvalho^{a,b,m,r}

^a Interdisciplinary Center for Archaeology and Evolution of Human Behaviour (ICArEHB), Universidade
do Algarve, Campus Gambelas, 80005-139, Faro, Portugal

^b Primate Models for Behavioural Evolution, Institute of Cognitive and Evolutionary Anthropology,
University of Oxford, 64 Banbury Road, Oxford, OX2 6PN, United Kingdom

^c GeoZentrum Nordbayern, Friedrich-Alexander-Universität Erlangen-Nürnberg, Schlossgarten 5,
91054 Erlangen, Germany

^d Institut für Geowissenschaften, Christian-Albrechts-Universität zu Kiel, Ludewig-Meyn-Str. 10,
24118 Kiel, Germany

^e Department of Human Evolution, Max Planck Institute for Evolutionary Anthropology, Deutscher
Platz 6, 04103 Leipzig, Germany

^f Department of Organismal Biology and Anatomy, University of Chicago, 1027 E. 57th St., Chicago, IL
60637, USA

^g Department of Archaeology, University of Cape Town, Private Bag X3, Rondebosch 7701, South
Africa

^h Evolutionary Studies Institute and School of Geosciences, University of the Witwatersrand, P Bag 3,
WITS 2050, South Africa

ⁱ Department of Zoology, University of Oxford, South Parks Road, Oxford OX1 3PS, United Kingdom

^j Center for the Advanced Study of Human Paleobiology, George Washington University, 800 22nd St
NW, Washington, DC 20052, USA

^k Centre for Functional Ecology, Department of Life Sciences, University of Coimbra, Calçada Martim
de Freitas, 3000-456 Coimbra, Portugal

^l Organisms and Environment Division, School of Biosciences, Cardiff University, Biomedical Sciences
Building, Museum Avenue, Cardiff, CF10 3AX, United Kingdom

^m CIBIO/InBio, Centro de Investigação em Biodiversidade e Recursos Genéticos, Universidade do
Porto, Rua Padre Armando Quintas 7, 4485-661 Vairão, Portugal

ⁿ Senckenberg Biodiversity and Climate Research Centre, Senckenberganlage 25, 60325 Frankfurt,
Germany

^o Department of Biomaterials and Biomimetics, New York University College of Dentistry, 345 East
24th Street, NY 10010, USA

^p Faculdade de Letras e Ciências Sociais, Universidade Eduardo Mondlane, Av. Julius Nyerere, 3453
Maputo, Mozambique

^q Programa de Antropología, Instituto de Sociología, Pontificia Universidad Católica de Chile, Av.
Vicuña Mackenna 4860, Macul, Santiago 6904411, Chile

^r Gorongosa National Park, Sofala, Mozambique

^s AESDA - Associação de Estudos Subterrâneos e Defesa do Ambiente, Portugal

^t National Science Foundation, 2415 Eisenhower Ave., Alexandria, VA, 22314, USA

* Corresponding author (Email: joerg.habermann@fau.de, Phone: +49 9131 8529026)

Abstract

The East African Rift System (EARS) has played a central role in our understanding of human origins
and vertebrate evolution in the late Cenozoic of Africa. However, the distribution of fossil sites along

the rift is highly biased toward its northern extent, and the types of paleoenvironments are primarily restricted to fluvial and lacustrine settings. Here we report the discovery of the first fossil sites from the Urema Rift at Gorongosa National Park (central Mozambique) at the southern end of the EARS, and reconstruct environmental contexts of the fossils. *In situ* and surface fossils from the lower member of the Mazamba Formation, estimated to be of Miocene age, comprise mammals, reptiles, fishes, invertebrates, palms, and dicot trees. Fossil and geological evidence indicates a coastal-plain paleoenvironmental mosaic of riverine forest/woodland and estuarine habitats that represent the first coastal biomes identified in the Neogene EARS context. Receiving continental sediment from source terranes west of today's Urema Graben, estuarine sequences accumulated prior to rifting as compound incised-valley fills on a low-gradient coastal plain following transgression. Modern environmental analogues are extremely productive habitats for marine and terrestrial fauna, including primates. Thus, our discoveries raise the possibility that the Miocene coastal landscapes of Gorongosa were ecologically-favorable habitats for primates, providing relatively stable maritime climate and ecosystem conditions, year-round freshwater availability, and food both from terrestrial and marine sources. The emerging fossil record from Gorongosa is beginning to fill an important gap in the paleobiogeography of Africa as no fossil sites of Neogene age have previously been reported from the southernmost part of the EARS. Furthermore, this unique window into past continental-margin ecosystems of central Mozambique may allow us to test key paleobiogeographic hypotheses during critical periods of primate evolution.

Keywords

Eastern Africa; continental margin; landscape reconstruction; depositional environments; paleontology; primate behavioral ecology

1 Introduction

Much of our understanding of vertebrate evolution and human origins in the late Cenozoic of Africa derives from Late Miocene and Pliocene fossil localities distributed along the East African Rift System (EARS) in Ethiopia, Kenya, Tanzania, and Malawi (e.g., Schrenk et al., 1993; Pickford and Senut, 2001; Harris and Leakey, 2003; Quade and Wynn, 2008; White et al., 2009; Harrison, 2011). However, no Neogene sites have yet been reported from the southernmost 1,000 km of the EARS. Furthermore, nearly all known EARS sites derive from fluvial and lacustrine settings. Here we report the first fossil sites from the Urema Rift in Gorongosa National Park (GNP), central Mozambique, at the southern end of the EARS (Fig. 1), and use the fossils, geological evidence, and stable isotopic composition of pedogenic carbonate to reconstruct environmental contexts. These sites, broadly attributed to the Miocene (Real, 1966; Grantham et al., 2011), fill a biogeographic gap between South and East African paleontological sites, and provide the first evidence of estuarine and coastal forest/woodland paleoenvironments of the EARS.

Sedimentary successions of the lower member of the Mazamba Formation (Fig. 2) were studied during two field seasons at GNP in 2016 and 2017. Fieldwork was conducted by the Paleo-Primate Project Gorongosa (PPPG), a multidisciplinary research initiative on human origins, initiated to unravel the evolutionary history of this relatively unexplored region. We compile comprehensive datasets using sedimentological logging and facies, petrographic, and geochemical analyses to provide a better understanding of the complex interactions between rift tectonics, relative sea-level changes, and the development of regional sedimentary environments. Combined with paleontological and paleoecological studies, these analyses are essential to (a) reveal the role of the Gorongosa area in the paleobiogeography of Africa, (b) enhance our knowledge on how rifting affected sedimentary systems and consequent faunal and floral evolution in the southern part of the EARS, and (c) assess the potential of the area for providing ecologically-favorable habitats for

primates during an as-yet poorly-documented key interval in the evolutionary history of African ecosystems (e.g., Cote, 2018; Kaya et al., 2018).

2 Geological setting and stratigraphy

EARS-related rifting initiated in Mozambique at $\sim 3 \pm 1$ Ma and led to the formation of the Urema Graben, the youngest and southernmost continental section of the EARS (Macgregor, 2015). Rift-shoulder uplift relative to graben subsidence resulted in the development of the modern physiography of the Bárue Platform with Mount Gorongosa in the west, the central Urema Graben, and the Cheringoma Plateau (rift-shoulder cuesta) in the east, exposing distinct lithostratigraphic successions (Fig. 2). Unconformably overlying Eocene marine limestones of the Cheringoma Formation on the Cheringoma Plateau are sedimentary successions that we herein refer to as Mazamba Formation. A review of the literature revealed inconsistencies in nomenclature and subdivision of this <130 m thick succession (cf., Real, 1966; Tinley, 1977; Lächelt, 2004; GTK Consortium, 2006; Steinbruch, 2010; Grantham et al., 2011; Pickford, 2013). Based on Real (1966), Tinley (1977) refers to the succession as Mazamba Formation (see also Steinbruch, 2010; Pickford, 2013), attributes it to a Mio-Pliocene age, and subdivides the formation into a basal member of red sandstone and quartzitic limestone, a central chert unit, and an upper quartzitic and conglomeratic Inhaminga sandstone member. By contrast, the geological explanations produced by the GTK Consortium (2006) and Grantham et al. (2011) subdivide the succession into two separate formations, including the basal Inhaminga Formation, estimated to be of Miocene age, and the overlying Mazamba Formation, tentatively reaching a Pliocene age. Our preliminary surveys suggest that the succession records an overall transgressive-regressive trend – in concert with existing literature data – and lacks clear lithostratigraphic criteria for the distinction of separate formations thus far. Hence, we herein use Mazamba Formation to collectively refer to this succession and differentiate a lower and an upper (Inhaminga) member (cf., Real, 1966; Tinley, 1977; Pickford,

2013). The lower member contains fossil wood and mammal remains, suggesting a terrestrial setting (Pickford, 2013), but also contains fossil marine mollusks, indicating a deltaic or marine environment (Real, 1966; Tinley, 1977; GTK Consortium, 2006; Grantham et al., 2011; Pickford, 2013). The upper member rarely contains fossils, and the facies has been interpreted as a transition from littoral to continental (Real, 1966; Tinley, 1977; GTK Consortium, 2006; Grantham et al., 2011).

3 Material and methods

3.1 Fieldwork

Fieldwork at GNP involved surveying of satellite imagery for potential rock exposures, helicopter air reconnaissance and ground surveys of targeted sites in the field, GPS positioning, geological mapping, detailed sedimentological logging, paleontological sampling, and collecting rock and pedogenic carbonate samples for subsequent laboratory analyses. To establish a systematic database, the Gorongosa area was geographically subdivided based on the major drainage network, and each sector was named according to its southern boundary river (labeled rivers in Fig. 2A). Sedimentary facies were studied using measured vertical sections that were logged to cm-scale accuracy. Directional transport indicators (channel orientations, grain fabrics, bedding structures) were measured to reconstruct paleocurrent directions. Directional values were corrected for -11° magnetic declination as local declination in the Muaredzi Sector in August 2016 was estimated at $10.81^\circ \text{ W} \pm 0.39^\circ$ using the most recent World Magnetic Model for calculation (<http://www.ngdc.noaa.gov/geomag-web/#declination>, accessed August 2016).

3.2 Geological rock samples

Geological rock samples were recovered from isolated exposures and from continuous measured sections for various analytical purposes. Sedimentary rocks were sampled for (a) petrographic thin-section and microfacies analyses using transmitted light microscopy, and (b)

paleontological analysis of contained invertebrate micro- and malacofauna applying sample-disaggregation techniques (H_2O_2 and Rewoquat treatment; Jarochowska et al., 2013), wet-sieving over 63 μm mesh sieves, and reflected light microscopy. To determine detrital modes of sandstones (mineralogical and modal compositions; texture of rock fragments) and maximize source-rock information, thin section samples were point counted using the Gazzi-Dickinson method (Gazzi, 1966; Dickinson, 1970). The term ‘wacke’ herein refers to sedimentary rocks with 15-75% matrix ($<30\ \mu\text{m}$) content (Dott, 1964; Pettijohn et al., 1973). Carbonate content in selected sediment samples was determined by the “Karbonat-Bombe” technique (Müller and Gastner, 1971).

3.3 Stable isotopic analysis

Pedogenic carbonate nodules were sampled for stable carbon and oxygen isotopic analysis (reported as $\delta^{13}\text{C}$ and $\delta^{18}\text{O}$ values). Stable isotope analysis of three carbonate samples was conducted at Goethe University and Senckenberg BiK-F Joint Stable Isotope Facility Frankfurt, Germany. Nodules were cut in two and powder was extracted from the center with a diamond tip dental drill. Untreated powders (180 to 2050 μg) were reacted with 99 % H_3PO_4 for 90 minutes at 72°C in continuous flow mode using a Thermo MAT 253 mass spectrometer interfaced with a Thermo GasBench II. Analytical procedures follow Spötl and Vennemann (2003). Carrara Marble with 2.01 ‰ VPDB ($\delta^{13}\text{C}$) and -1.74 ‰ VPDB ($\delta^{18}\text{O}$) was used as internal laboratory standard for calibration. Final isotopic ratios are reported against VPDB ($\delta^{13}\text{C}$) and VSMOW ($\delta^{18}\text{O}$); overall analytical uncertainties are better than 0.04 ‰ and 0.07 ‰, respectively.

4 Results

4.1 Study areas

The study areas are situated in the central Muaredzi Sector on the Cheringoma Plateau (Fig. 2A, C). Apart from Menguere Hill, a sub-circular hill ~3.5 km west of GPL-1 that rises ~40 m above its

surroundings, the region exhibits elevations between ~100-120 m a.s.l. Rock exposures, most commonly provided by incised gullies at head regions of small tributary channels or by channel flanks, are highly localized due to dense ground vegetation. Stratigraphic sections were measured wherever possible, including the key localities GPL-1 (SW and NE), GPL-2, GPL-6, GPL-8, and GPL-9 (Figs. 2C, 3).

4.2 Facies associations, petrography, and paleocurrent data

The lower Mazamba successions at the southern sites (GPL-1, GPL-6, GPL-7, GPL-8) are dominated by basal conglomeratic and sandy facies assemblages overlain by clayey sandstones to wackes and sandy clay- and marlstone units (Fig. 3). By contrast, the northeastern sites, representing laterally correlative (GPL-9) and younger stratigraphic levels (GPL-2, GPL-3), are sand dominated and contain a rich marine invertebrate fossil record. The GPL-1SW section starts at the base with an at least 13 cm thick (base not exposed) unit of massive sandy claystones (Facies 1). Unconformably overlying the erosional surface truncating this unit is a 90 cm thick succession of well-lithified, sparry calcite-cemented, feldspatho-quartzose granule conglomerate to coarse sandstones (Facies 2; Table 1, Appendix A, Figs. 4A-C, 5B). The conglomerate- and sand-bodies display broad and shallow channel morphologies, contain basal and internal truncation surfaces, and exhibit low-angle and trough-cross-bedding and well-defined fining-upward trends within individual beds. Laterally towards GPL-8, this unit passes into granule to pebble conglomerates that are dominated by siliciclastic lithologies but also contain fossil oysters and bioclastic debris towards the top of the unit. Similar conglomerates at this stratigraphic level were discontinuously traced over almost 3 km northeast to GPL-9 (e.g., Fig. 5A) where further bioclastic constituents, including fragments of mollusk shells (Fig. 5J), corallinacean red algae (Fig. 5K), and serpulid worm tubes (Fig. 5L), occur towards the top of the conglomeratic bottom facies. What follows above at GPL-1-GPL-6 is a <80 cm thick unit of poorly-sorted, medium- to coarse-grained wackes with upwards increasing (35-64 vol.%) matrix contents

(Facies 3). This unit is massive to crudely stratified and rich in fossil vertebrate remains. Mottling and reddening, rhizoliths (subvertical, downwards tapering, clay-filled root casts, <2 mm wide and <4 cm long), bioturbation, and scattered carbonate nodules suggest prolonged periods of landscape stability, hiatuses in deposition, and pedogenic overprinting. Matrix and lime mud contents increase while grain-sizes decrease upsection, and the wackes of Facies 3 grade into calcareous sandy clay- and mudstones of Facies 4. This unit is <1 m thick and contains sand and carbonate nodules at GPL-1, while relatively pure, waxy claystones are exposed at GPL-6. Overlying a sharp, erosional contact truncating the claystones of Facies 4 is a massive unit of clayey sandstones to wackes (Facies 5), which, in turn, is topped by sandy clay- to marlstones of Facies 6. In contrast to Facies 4, this unit contains significant amounts of lime mud (between 25-39 % CaCO₃; Table 1, Appendix A) and fossil shark tooth fragments. Thin (<1 cm) sand lenses, interleaved laterally and vertically with massive, sandy clay- and marlstones of Facies 4 and 6, occur sporadically. Abundant limestone nodules, calcareous root and/or burrow casts, and large fossil vertebrate remains (e.g., Fig. 6) associated with at least three stratigraphic levels in the upper GPL-1 succession (Fig. 3) may indicate repeated emergence and pedogenic overprinting. At GPL-6, the claystones of Facies 6 are erosionally capped by well-sorted, low-angle cross-bedded quartzitic sandstones with common clay clasts demarcating internal truncation surfaces (Facies 7), which are considered correlative with the basal facies exposed at GPL-2 based on facies characteristics. Six facies are distinguished in the sand-dominated GPL-2 succession above, including two fossiliferous beds rich in marine oysters, gastropods, and crustacean remains (Facies 8 and 11; Figs. 3, 7). Above the sandstones of Facies 11 follows another <70 cm thick claystone unit (Facies 12), which is erosionally overlain by heavily rooted, quartzitic sandstones (Facies 13) that comprise the top of the GPL-2 succession. In summary, the studied successions (a) are erosionally-based (unconformity-bound) above a basal claystone (Facies 1), (b) describe an initial fining upward trend (Facies 2-4), (c) contain sediment from two distinct sources (extrabasinal siliciclastics vs. intrabasinal lime mud and bioclastics), (d) are dominated in the central section (Facies

3-6) by muddy sediments, and (e) are capped by invertebrate-rich, sandy successions at GPL-2 and GPL-3 (Facies 7-13).

Bulk-sediment petrographic data (Table 1, Appendix A) were obtained to assess sandstone provenance (e.g., Garzanti, 2016). According to their main components (Fig. 4A, B) and overall modal compositions (Fig. 4C), rock samples classify as feldspatho-quartzose to quartzose, plutoniclastic granule-conglomerates, sandstones, wackes, and sandy clay- and marlstones containing minor amounts of metamorphic material. Sand fractions in all samples analyzed are dominated by quartz with <59 vol.% (Figs. 4C, 5). Quartzes are commonly sub-rounded and, in order of decreasing abundance, mainly occur as (a) strained mono crystals with undulose extinction, (b) sand-sized, strained crystals within larger plutoniclastic granite fragments (Fig. 5H-J), and (c) mono crystals with constant to slightly undulatory extinction. Undulose extinction of quartz grains indicates strain and crystal plastic deformation during granite emplacement (Phillips, 1965; Caracciolo et al., 2012). Feldspar occurs with ~<12 vol.%, with alkali feldspar being consistently more abundant than plagioclase. Similar to quartz, feldspars are commonly sub-rounded and occur as single crystals or as sand-sized crystals within plutoniclastic granite fragments. Myrmekitic quartz-feldspar intergrowths, feldspar leaching and sericitization are common; few grains also display internal deformation features including undulatory extinction. In addition to plutoniclastic rock fragments occur minor amounts of lithic clasts of fine-grained dolerite, rare chert, clay clasts, and metamorphic rock-fragment types (displaying, e.g., subtle foliation, sutured grain boundaries, subgrains, and subgrain rotation due to crystal plastic deformation). Wackes with matrix contents exceeding 15 vol.% (Table 1, Appendix A, Figs. 4C, 5M-O) and sandy clay- and marlstones towards the top of the GPL-1 section contain considerable amounts of lime mud (between 25-39 %; Table 1, Appendix A, Fig. 4C). Accessory constituents comprise biotite, muscovite, and a heavy mineral assemblage dominated by opaque oxides, zircon, tourmaline, rutile, and rare garnet. Invertebrate fossils and bioclastic detritus

(e.g., Figs. 5J-L, 7) are restricted to the upper parts of the basal conglomerates and sandstones at GPL-8 and GPL-9 (Facies 2) and to the succession at GPL-2 and GPL-3 (Facies 8 and 11).

Paleocurrent indicators were documented at several localities from fluvial deposits of the Mazamba Formation (Table 2, Appendix B). They demonstrate a fairly consistent pattern, predominantly revealing ENE-directed paleotransport (Fig. 4D) that suggests sediment sources west of today's Urema Graben.

4.3 Paleosols and stable isotope data

The main diagnostic pedogenic features observed at various levels in the studied successions are Bk horizons associated with mottling, rhizoliths, bioturbation, and nodular carbonate. Carbonate glaebules range from diffuse, early-stage nodules to well-consolidated concretions <3 cm in diameter. The latter are generally massive with distinct boundaries, indicating finely distributed carbonate leached from overlying soil horizons (Wieder and Yaalon, 1982). Here we present the first paleoecological analysis of pedogenic carbonates from the southernmost EARS, using stable carbon and oxygen isotope analyses to reconstruct past vegetation cover (C_3 vs. C_4 biomass) and hydrological processes. We analyzed three carbonate nodules from a paleosol Bk horizon in the basal fluvial section (Facies 2) at GPL-1SW (Fig. 3). $\delta^{13}C$ values are -10.2, -9.6, and -9.0 ‰ (mean = -9.6 ‰, σ = 0.6 ‰), while $\delta^{18}O$ values are 23.6, 23.2, and 23.0 ‰ (mean = 23.2 ‰, σ = 0.3 ‰), respectively. For complete stable isotope results, including calibration standards, refer to Appendix C.

4.4 Fossil vertebrate fauna

Two field seasons of paleontological survey at GNP have resulted in 157 vertebrate specimens (e.g., Fig. 6), including the first dentognathic fossils ever reported from this part of the EARS. The fossils derive from eight localities, but GPL-1 (Figs. 2C, 3) has yielded 84 % of the specimens. Each locality was systematically surveyed and surface specimens were collected. Most *in situ* fossils were

excavated using standard paleontological techniques to record contextual sedimentary and chronostratigraphic information (e.g., Behrensmeyer and Barry, 2005). Mammals are more abundant than other vertebrates, but most specimens are fragmentary postcranial elements and fragments of tooth enamel. The larger postcranial elements (e.g., scapular glenoid fragment, distal humerus, distal radius, carpal bones, vertebrae and sacrum fragments, acetabulum, femoral head) likely belong to species of Proboscidea (Fig. 6B). Several tooth enamel fragments provide evidence of brachyodont mammals with thin enamel. Two complete tooth crowns have been found: a suid upper incisor from GPL-1 (Fig. 6D), and a likely sivathere incisor from GPL-2. Other fossils include crocodile tooth fragments, chelonian carapace and plastron fragments, and a shark tooth fragment (Fig. 6C). Overall, these localities show a taphonomic bias towards the preservation of larger vertebrates (proboscidean or hippopotamus size), although some medium-sized vertebrates (e.g., suids) are also preserved. No micromammals have been recovered yet.

4.5 Fossil invertebrate fauna

An oyster valve, attributed to *Striostrea margaritacea*, was found along with other bioclastic (mainly mollusk) debris towards the top of Facies 2 at GPL-8 (Fig. 3). Mollusk debris (Fig. 5J) and additional corallinacean red algae (Fig. 5K) and serpulid worm tubes fragments (Fig. 5L) are also common towards the top of the conglomerate at GPL-9, which is considered correlative based on facies characteristics. Stratigraphically younger levels at GPL-2 have yielded rich remains of crustaceans, gastropods, and bivalves that were found *in situ* or weathered out of the sandstones of Facies 11 (Fig. 3). Decapod crustaceans are represented by a fragmentary left propodus and two isolated left dactyli (Fig. 7.1-4). The propodus belonged to a ghost shrimp of the family Callianassidae. The dactyli cannot be identified, but most likely are conspecific with the propodus. The fossil gastropod fauna is dominated by members of the family Cerithiidae (Fig. 7.8-13; e.g., Kilburn and Rippey, 1982). The poorly preserved shell fragments belong to a series of taxa, e.g., the

genus *Rhinoclavis* (Fig. 7.13). One gastropod shell (Fig. 7.5-7) shows a nearly completely abraded outer surface, with only faint spiral lines visible at its base, and has a characteristic oval outline in apical view. It resembles *Terebralia palustris* in general morphology (e.g., Kilburn and Rippey, 1982), but the lack of ornamentation prevents reliable identification. Bivalves are represented by oyster shells, mostly identified as *Striostrea margaritacea* (Fig. 7.16-27; Kilburn and Rippey, 1982). One left valve described herein as *Striostrea* sp. (Fig. 7.14-15) shows radial ribs, thereby resembling *Saccostrea cucullata*; however, this species is smaller and has a folded commissure not visible in the present specimen. Characteristic are traces of barnacle attachments on the oyster shells (e.g., Fig. 7.23-25). One specimen exhibits a drill hole with vertical sides most likely caused by a carnivorous muricid gastropod (Fig. 7.25-27; compare Hoffman et al., 1974).

4.6 Fossil flora from Menguere Hill

Several sites on the western footslope of Menguere Hill (Fig. 2C), which had been noted by Pickford (2013), have yielded large silicified tree trunks and smaller wood fragments scattered on the ground surface. One piece was the base of a large palm tree (Fig. 8A), recognized by the remnant cluster of roots (Fig. 8B). There were two other large trunks, each comprising several sections, the first with a diameter of 1.6 m (Fig. 8C) and the second just over 1 m (Fig. 8D). Most of the large trunks had bark preserved (Fig. 8C). Based on hand specimens it seems that there are at least four types of dicot wood and one palm tree. Microscopic studies of thin-sectioned wood samples (Fig. 8E, F) enable their identification to genus or species level based on wood anatomical features. One sample is an angiosperm or hard wood (Fig. 8D-G), most likely a member of the family Combretaceae and the genus *Terminalioxylon*. The large and very low density vessels indicate that the wood is very mesophytic and cannot tolerate water stress (Carlquist, 1975).

5 Discussion

5.1 Sediment provenance and age constraints

Detrital modes of sediments from the lower member of the Mazamba Formation (Fig. 4B) indicate a continental block provenance (Dickinson, 1985) and erosional unroofing of continental crust (e.g., Garzanti, 2016). Revealed by the dominance of granitic rock-fragment types (Fig. 5G-J), the felsic plutonic rocks of the Gorongosa Suite (Fig. 2A, B) are considered as dominant source terrain for siliciclastic detritus (Fig. 9). Bulk sediment petrographic data reveals extensive overlap between the studied deposits and modern sands (orogenic and anorogenic) generated along the South African passive continental margin (Fig. 4B; Garzanti, 2016). However, marked similarities also occur with sands of dissected continental block provenance from the EARS, which are strictly controlled by climate-related weathering (Garzanti, 2016). In this light, sandstone compositions may reflect weathering trends in intermediate conditions between wet equatorial and tropical dry contexts.

Enhanced thicknesses of Mazamba deposits in the central rift relative to the eastern rift-shoulder, as indicated by Lächelt (2004; Fig. 2B), may reflect source-ward E-W thickening trends if sedimentation occurred prior to rifting, or may imply synsedimentary faulting (differential sedimentation rates across fault compartments) and early syn-rift deposition. However, reduced sedimentation, non-deposition, and/or erosion would have been the dominant processes in footwall settings with progressive rift-shoulder uplift from $\sim 3 \pm 1$ Ma onwards (Macgregor, 2015), implying that sedimentation initiated prior to rifting in the Miocene (cf., Real, 1966; Tinley, 1977; Steinbruch, 2010). In conclusion, lateral E-W thickness variations (Fig. 2B), bulk sediment petrography (Table 1, Appendix A, Figs. 4A-C, 5), and eastward-directed paleocurrents (Table 2, Appendix B, Fig. 4D) indicate that the lower member of the Mazamba Formation was dominantly shed from granitic source terrains west of today's Urema Graben (Fig. 9) and a pre-rift age $> 3 \pm 1$ Ma.

5.2 Depositional environments

Sedimentary facies, facies architecture, and sediments both from terrestrial (extrabasinal siliciclastics) and marine sources (intrabasinal marlstones and bioclastics) indicate a coastal estuarine depositional context for the GPL successions (e.g., Dalrymple et al., 1992; Boyd et al., 2006; Figs. 3, 9). By definition, estuaries occupy the seaward portion of drowned valley systems, receive sediment both from fluvial and marine sources, and contain facies influenced by tide, wave, and fluvial processes (Dalrymple et al., 1992). Wave-dominated estuaries typically exhibit a tripartite subdivision including (a) high-energy, alluvial and bay-head delta facies assemblages in the river-dominated realm, (b) organic-rich muds formed under low- to mixed-energy conditions in the central basin, and (c) high-energy, marine shoreface, barrier, and shelf deposits in the seaward portion of the estuary (Dalrymple et al., 1992; Zaitlin et al., 1994; Boyd et al., 2006). As estuarine systems are transgressive in nature, their stratigraphic architecture is characterized by vertical stacking of these facies assemblages as sea level rises (Boyd et al., 2006). Grain-size, sorting, and fabric characteristics of conglomerates and sandstones of Facies 2 (Fig. 3) suggest formation in the upper flow regime during late lowstand to early transgressive phases, with channel geometries and bedding features typical of bedload-dominated, shallow drainages (Miall, 2006). Underlying claystones of Facies 1, instead, indicate deposition from suspension under low-energy conditions, tentatively attributable to fluvial overbank or central-basin estuarine environments. Their bounding unconformity and superimposed fluvial facies suggest a compound valley-fill scenario (e.g., Zaitlin et al., 1994), in which the overall transgressive trend has been accentuated by smaller-scale base-level fluctuations resulting in multiple cycles of incision and deposition and vertical stacking of fluvial and estuarine facies (e.g., Clark and Reinson, 1990; Plink-Björklund, 2005). Marine invertebrate fossils towards the top of Facies 2 at GPL-8 suggest reworking and admixture of bioclastic detritus as relative sea level rises and the shoreline transgresses (Zaitlin et al., 1994). Following further base-level rise, documented by upwards decreasing grain sizes (fining upward) and increasing mud contents, the overlying wackes of Facies 3 formed as river discharge and fluvial sediment input continued.

373 Together with the vertebrate record from this level and evidence for emergence and pedogenesis,
374 Facies 3 is interpreted as bayhead delta assemblage. The deepening trend continues above, so that
375 the sandy clay and marlstone, including shark remains, of Facies 4 and 6 accumulated as estuarine
376 and/or swamp muds under low- to mixed-energy conditions in the inner (central basin) and/or
377 marginal (mangrove swamp?) estuary (Allen and Posamentier, 1994; Boyd et al., 2006). Occasional
378 emergence and pedogenesis of what is considered here the central-basin facies may particularly be
379 the case when taking into account the relatively small scale (<6 km across) and shallow depths of
380 modern, wave-dominated estuarine systems at the Cheringoma Coast. These are highly dynamic
381 environments prone to frequent modifications from fluctuating river run-off, avulsion (e.g., Facies 5),
382 desiccation, and wave- or tide-induced processes. Large vertebrate remains found *in situ* at multiple
383 levels in this part of the succession at GPL-1 (Facies 4 and 6) support the inference of shallow central-
384 basin to marginal swamp environments. Sedimentary facies (e.g., tidal bedding with mud drapes,
385 transgressive lag, tempestite) of sand-dominated, younger successions (Facies 7-11) at GPL-6 and
386 GPL-2, together with the rich invertebrate fauna from GPL-2, indicate shallow-marine conditions and
387 highstand deposition (transgressive shoreface, barrier, lagoonal, and shelf deposits). Embayed to
388 lagoonal environments with brackish water conditions, which typically occur in estuaries (Boyd et al.,
389 2006), are evident from invertebrate autecology. The concentration of disarticulated oyster shells in
390 Facies 11 implies an allochthonous origin and possibly storm-induced resedimentation. Their chaotic
391 orientation can be explained by redistribution (bioturbation) by burrowing, infaunal organisms after
392 the storm event. The claystones above (Facies 12) may indicate recurring estuarine central-basin
393 conditions due to continued river discharge and sea-level fluctuations. Based on the facies
394 assemblages described above and their stratigraphic architecture, we interpret the studied
395 succession as an estuarine depositional complex (Figs. 3, 9). An incised valley-fill scenario (e.g., Zaitlin
396 et al., 1994) is conceivable when considering the major unconformity between the Eocene marine
397 Cheringoma Formation and overlying fluvial deposits of the Miocene Mazamba Formation. As such,

incised valleys and erosional surfaces formed by fluvial incision when the base level was lowered by falling sea levels after the Eocene. With a rising sea level, estuarine sequences accumulated as compound incised-valley fills (e.g., Allen and Posamentier, 1994; Boyd et al., 2006) on an incised low-gradient coastal plain superimposed on this subaerial unconformity.

Menguere Hill, ~3.5 km west of GPL-1 (Fig. 2C), exposes a series of silicified limestone beds halfway up its western slope. Mudcracks, indicating surface exposure, had previously been noted, and the beds have been interpreted as paleo-pan deposits (abandoned oxbows, small coastal-plain lakes; Pickford, 2013). Lamination is common and is typical of pedogenic calcretes/silcretes, although lacustrine/palustrine processes are commonly involved along pan margins (Mees, 2002). Meandering rivers and oxbow lakes typically characterize low-gradient coastal plains (e.g., Miall, 2006), and, together with oval pans, are also common landscape features of the Cheringoma Coast today (Tinley, 1977). Together with the fossil flora, the Menguere Hill succession is interpreted as a riverine forest/woodland paleoenvironmental mosaic and is considered as correlative inland equivalent to the estuarine GPL sites based on similar elevation (Figs. 3, 9).

5.3 Stable isotopic composition of pedogenic carbonates

Stable isotopic composition of carbonate nodules from the fluvial paleosol at GPL-1SW (Figs. 2C, 3) reflects a closed woodland habitat with a vegetation dominated by C₃ biomass (e.g., dicot trees and palms), and relatively little effects of soil-water evaporation. The fraction of woody cover ranges between 65-74 % (after Cerling et al., 2011). Similar geochemical reconstructions of Mio-Pleistocene woody cover in the EARS are biased towards sites in its northern extent, and point towards a prevalence of open savanna habitats with <40 % woody cover at most sites (e.g., Ségalen et al, 2007; Cerling et al., 2011). By contrast, the Plio-Pleistocene deltaic deposits of the Karonga Basin hominin site (Malawi Rift), the closest hominin locality to GNP in the rift, reflect a persistent wooded environment with ~60-70 % woody cover in a mosaic habitat (Lüdecke et al., 2016a, b). This is similar

to what we deduce for the GNP site, but may be partly due to the older Miocene age estimated for the GNP site - a period when closed woodland habitats were more widespread in the EARS (e.g., Cerling et al., 2011; deMenocal, 2011).

5.4 Paleoecology

Fossil vertebrate remains (e.g., Fig. 6) from GPL-1 (Figs. 2C, 3) show a mix of terrestrial (suids, proboscideans) and aquatic fauna (crocodiles, turtles, shark), which is consistent with the estuarine setting reconstruction provided on sedimentological grounds. The recovered fragments of enamel are indicative of brachyodont dentitions, i.e., derived from browsing mammals with a relatively soft diet likely in closed or wooded environments. There are no indications of hypsodont teeth among the mammalian specimens. This supports a paleoecological reconstruction whereby grasses are relatively underrepresented in the Gorongosa ecosystem. Postcranial elements are too fragmentary for ecomorphological analyses.

The fossil invertebrate fauna (Fig. 7) from GPL-2 (Figs. 2C, 3) represents a marginal-marine setting of low to moderate diversity. Almost all callianassid crustaceans live in burrow systems in sandy to muddy substrates of shallow-marine environments (e.g., shallow bays and lagoons; Murphy and Kremer, 1992). Most taxa feed on detrital matter entering the burrows or organic particles within the sediment (e.g., algae; Murphy and Kremer, 1992). Gastropod shells are dominated by elements of the family Cerithiidae. Members of this diverse, mainly tropical family are predominantly herbivores feeding on algae or organic debris, and prefer protected habitats with fine-grained substrates, such as lagoons or bays (Kilburn and Rippey, 1982). A single specimen has been tentatively assigned to *Terebralia palustris* (Potamididae). Poor preservation precludes a definitive identification, yet it should be noted that *Terebralia palustris* is typical for muddy or sandy substrates in bays and lagoons, particularly in the vicinity of mangroves where it can tolerate wide salinity fluctuations and even subaerial exposures (Kilburn and Rippey, 1982; Branch et al., 2002). The

bivalve fauna is dominated by *Striostrea margaritacea*, which is known to form beds in sandy to rocky areas of the tidal zone, often in areas of high wave energy (Kilburn and Rippey, 1982; Branch et al., 2002). It is known to have a high tolerance to salinity fluctuations and is also found within estuaries characterized by brackish water conditions (Kilburn and Rippey, 1982). A marine influence is also visible by the barnacles and by the bored oyster shell, an indication for the presence of muricid gastropods. Barnacles and muricid gastropods mostly occur in marine shallow-water habitats. While barnacles are known to tolerate adverse conditions such as subaerial exposure in tidal areas, comparatively few muricid species can tolerate brackish environments.

The genus *Terminalioxylon* (Fig. 8D-G) in the fossil flora from Menguere Hill (Fig. 2C) indicates a mesophytic habitat, with large palm and dicot trees growing under well-drained soil conditions with low water stress (e.g., Carlquist, 1975). These conditions contrast with the estuarine context at GPL-1, where water-logged substrates and swamp conditions are predicted. Well-drained parts of paleolandscapes in the coastal hinterland may comprise gravel-sand substrates of interfluvies, emerged sandy bars and ridges, or paleopan margins on a coastal floodplain dominated by shallow gravel-sand meandering rivers (e.g., Miall, 2006). This context, together with the floral assemblage, suggests a riverine forest/woodland paleoenvironmental mosaic at Menguere Hill that grades eastwards into nearshore habitats (Fig. 9).

Orographic and maritime control of rainfall regimes are considered to have had a strong amelioration effect on coastal paleoenvironments of central Mozambique (e.g., Tinley, 1977; Burke and Gunnell, 2008). Mio-Pliocene sea-surface currents and littoral wave/tide regimes offshore central Mozambique are expected to have been comparable to today due to the already-established Indian Ocean Monsoon (deMenocal, 1995) and Mozambique Current (Schlüter and Uenzelmann-Neben, 2007; Uenzelmann-Neben et al., 2007) and a similarly broad and shallow paleoshelf (Salman and Abdula, 1995). Strong, year-round orographic rains caused by ascent of moist air advected from the Indian Ocean to the rim of an uplifted hinterland plateau at >2,000 m a.s.l. (Tinley, 1977;

Partridge, 1997), hosting also Mount Gorongosa, should have released perennial streams that crossed the continental plain to the coast (Fig. 9). The combined maritime and orographic influences are thus considered to have had profound effects on climate and ecosystem stability in the Miocene of Gorongosa, in contrast to other EARS sites, where more variable continental climate prevailed (e.g., Nicholson 1996; Hély et al., 2006). Important paleoecological implications for coastal fauna likely include sustained availability of freshwater and food resources, and ecosystem conditions stable enough to make these habitats year-round refuges.

5.5 Primate coastal behavioral ecology: significance and potential

Although primates have not yet been recovered from the Gorongosa fossil record, modern ecological evidence suggests that the Miocene coastal landscapes of Gorongosa (Fig. 9) may have been ecologically attractive to them. Furthermore, major biogeographic gaps between East and South African hominin sites and the narrow range of depositional environments of EARS sites have made it difficult to test key hypotheses about the biogeography of human origins, e.g., the coastal forest hypothesis of Kingdon (2003), or the delta hypothesis of Wrangham (2005). The former hypothesis predicts that hominoids originated in coastal forest settings (see also Joordens, 2011), while the latter emphasizes that deltaic components of aquatic habitats may have been particularly important. The environmental stability of coastal forests has been well established for the Pleistocene (Couvreur et al., 2008), as has their role as refugia during periods of aridity (Kingdon, 2003; Joordens, 2011). Despite the lack of systematic studies on primate aquatic behavioral ecology, at least 30 species of extant non-human primates exploit aquatic resources in a variety of habitats, including riverine, deltaic, and estuarine environments (Kempf, 2009). The significance of such habitats in primate and hominoid evolution has been the subject of debates - the archeology of aquatic adaptation (Erlandson, 2001) - which continue largely unsolved due to the absence of East African fossil sites in Mio-Pliocene coastal forests. Our palaeoecological reconstruction of fossil sites

in coastal contexts will provide key data to evaluate hypotheses regarding the capacity of such habitats to drive primate evolution. Did hominoids evolve in coastal settings (Kingdon, 2003; Joordens, 2011), and were these marginal ecosystems, which Erlandson (2001) called “Gates of Hell”, operating as fallback ranging areas exploited predominantly by specialist primates, or were they the “Gardens of Eden”, preferentially selected by generalist primates (Erlandson, 1994, 2001)? Extant primates use aquatic habitats predominantly for thermoregulation, during social displays, in range expansion, as sources of food (both fauna and flora), and as refuges against predators and conspecific aggression (Kempf, 2009). Although these areas are not risk-free, harboring potential predators as well as water-borne diseases/parasites, they offer unique resources (e.g., aquatic foods containing high amounts of DHA, EPA, vitamin D, and micronutrients), which are thought to have a strong positive impact on human physiology and brain growth (Joordens, 2011). Importantly, these coastal forests may have hosted conditions that favored the origins and diversification of tool use suited to aquatic resources. Examples of stone-tool use to access seafood by long tailed macaques or by capuchin monkeys (Fernandes, 1991; Malaivijitnond et al., 2007; Luncz et al., 2017), and chimpanzees fishing for algae (Humle and Matsuzawa, 2009) validate this idea. Also, such environments are a host to other resources in aquatic environments that can be accessed with little to no technology (e.g., Archer et al., 2014). The absence or presence of primates at the Gorongosa fossil sites will be key to test Kingdon’s (2003) and Erlandson’s (1994, 2001) models of primate evolution in coastal forests.

6 Conclusions

Our interdisciplinary research provides new insights into the evolution of this minimally-explored region and resulted in the discovery of the first fossil sites from the Urema Rift that significantly extend our paleoenvironmental purview on the southernmost part of the EARS and underline the paleontological potential of the Gorongosa area. *In situ* and surface fossils from the lower member of

the Mazamba Formation comprise mammals, reptiles, fishes, invertebrates, dicot trees, and palms. Regional stratigraphic relationships, sedimentary facies, facies architecture, and the emerging fossil record suggest a paleoenvironmental mosaic of estuarine and riverine forest/woodland systems, which represent the first Miocene coastal habitats identified in the EARS. Receiving continental sediment from source terranes west of today's Urema Graben, estuarine sequences accumulated prior to rifting as compound incised-valley fills on a low-gradient coastal plain following transgression. Stable isotopic analyses of pedogenic carbonates from the fluvial part of the succession indicate a woody cover of 65-74 %, consistent with contemporaneous forest/woodland environments identified farther inland. Although we postulate a pre-rift scenario and reconstruct environments that should have been and still are widespread along the East African coast, it is only through rifting, regional uplift, and subsequent exposure of the Mazamba Formation that provide us with this unique window into past continental-margin ecosystems of central Mozambique. Today, such coastal systems are extremely productive habitats for marine and terrestrial fauna, including primates, and they may have had a similar habitat function in the past. Thus, our discoveries suggest that the coastal landscapes of Gorongosa were ecologically-attractive habitats for primates, providing relatively stable maritime climate and ecosystem conditions, year-round freshwater availability due to the combined maritime and orographic influences on rainfall regimes, and food both from terrestrial and marine sources. Especially in times when more continental environments would have been exposed to more severe oscillations in resource availability, these habitats may have served as year-round refuges. Together with the key position of GNP in a geographic gap bridging South and East African paleontological sites, we consider this region promising for understanding primate evolution, adaptation, paleobiogeography, and paleoecology. The need for more fossils to fill major gaps in the African paleontological record has recently been emphasized (Cote, 2018; Kaya et al., 2018). The emerging fossil record from Gorongosa will help fill these gaps and stresses the importance of understanding the evolutionary significance of regional

paleoenvironmental variability in Africa. Further research at GNP, including dating and multi-proxy analyses to contextualize past and recent conditions, is indispensable and will provide finer chronostratigraphic and environmental constraints. The presence or absence of primates in the fossil record from Gorongosa will be key for testing paleobiogeographic hypotheses of primate evolution. The integrated approach of the PPPG will also help structure our understanding of the ancient East African margin, Neogene climate and sea-level histories, rift evolution, and their intricate relationships and environmental impact in general.

Acknowledgments

The Paleo-Primate Project Gorongosa would like to thank the Gorongosa Restoration Project for the generous support with starting this interdisciplinary endeavor. This work was also supported by the National Geographic Society [grant number GEFNE169-16], the John Fell Fund [grant number 153/086], and a Philip Leverhulme Prize to Susana Carvalho [grant number PLP-2016-114]. Our work is only possible due to the visionary approach of Greg Carr and the dedicated staff from Gorongosa National Park, guided by Dr. Mateus Mutemba. We are very grateful to Dr. Solange Macamo, Dr. Mussa Raja at Universidade Eduardo Mondlane, and to all the Park "fiscais", to our students, and colleagues across many institutions who have been very enthusiastic about this project. J.M.H. benefitted from a grant provided by the Foundation for Science and Technology (FCT-Portugal), and acknowledges support by Nuno Bicho, Helga de Wall, Michel Bestmann, Lars Scharfenberg, Luca Caracciolo, and Harald Stollhofen. T.L. acknowledges funding by DFG grant LU 2199/1-1 and the laboratory support of Jens Fiebig. We further thank George Branch and Matus Hyzny for support in the identifications of invertebrate fossils, and Kathy Stewart for help with identifying fossil fish. C.C. is grateful for support by St. Hugh's College, University of Oxford.

Data Availability

The authors declare that all data supporting the findings of this study are included in the article and its supplementary information files.

References

Allen, G.P., Posamentier, H.W., 1994. Transgressive facies and sequence architecture in mixed tide- and wave-dominated incised valleys: example from the Gironde estuary, France, in: Dalrymple, R.W., Boyd, R.J., Zaitlin, B.A. (Eds.), *Incised-Valley Systems: Origin and Sedimentary Sequences*. SEPM Spec. Publ. 51, Tulsa, pp. 225–240.

Archer, W., Braun, D.R., Harris, J.W., McCoy, J.T., Richmond, B.G., 2014. Early Pleistocene aquatic resource use in the Turkana Basin. *J. Hum. Evol.* 77, 74–87.

Behrensmeyer, A.K., Barry, J.C., 2005. Biostratigraphic surveys in the Siwaliks of Pakistan: a method for standardized surface sampling of the vertebrate fossil record. *Palaeontol. Electron.* 8, 1-24.

Boyd, R., Dalrymple, R.W., Zaitlin, B.A., 2006. Estuarine and incised-valley facies models. *SEPM Spec. Publ.* 84, 171–235.

Branch, G.M., Griffiths, C.L., Branch, M.L., Beckley, L.E., 2002. *Two Oceans – A Guide to the Marine Life of Southern Africa*, fifth ed. David Philip, Cape Town.

Burke, K., Gunnell, Y., 2008. *The African Erosion Surface: A Continental-Scale Synthesis of Geomorphology, Tectonics, and Environmental Change over the Past 180 Million Years*. *Geol. Soc. Am. Mem.* 201, Boulder.

Caracciolo, L., Tolosana-Delgado, R., Le Pera, E., von Eynatten, H., Arribas, J., Tarquini, S., 2012. Influence of granitoid textural parameters on sediment composition: Implications for sediment generation. *Sediment. Geol.* 280, 93–107.

Carlquist, S., 1975. *Ecological Strategies of Xylem Evolution*. University of California Press, Berkeley.

596 Cerling, T.E., Wynn, J.G., Andanje, S.A., Bird, M.I., Korir, D.K., Mace, W., Macharia, A.N., Quade J.,
 597 Remien, C.G., 2011. Woody cover and hominin environments in the past 6 Million years. *Nature*
 598 476, 51–56.

599 Clark, J.E., Reinson, G.E., 1990. Continuity and performance of an estuarine reservoir, Crystal Field,
 600 Alberta, Canada, in: Barwis, J.H., McPherson, J.G., Studlick, J.R.J. (Eds.), *Sandstone Petroleum*
 601 *Reservoirs*. Springer, New York, pp. 343–361.

602 Cote, S., 2018. Savannah savvy. *Nat. Ecol. Evol.* 2, 210–211.

603 Couvreur, T.L.P., Chatrou, L.W., Sosef, M.S.M., Richardson, J.R.E., 2008. Molecular phylogenetics
 604 reveal multiple tertiary vicariance origins of the African rain-forest trees. *BMC Biol.* 6:54.
 605 DOI:10.1186/1741-7007-6-54

606 Crook, K.A.W., 1960. Classification of arenites. *Am. J. Sci.* 258, 419–428.

607 Dalrymple, R.W., Zaitlin, B.A., Boyd, R., 1992. Estuarine facies models: conceptual basis and
 608 stratigraphic implications. *J. Sediment. Petrol.* 62, 1130–1146.

609 deMenocal, P.B., 1995. Plio-Pleistocene African climate. *Science* 270, 53–59.

610 deMenocal, P.B., 2011. Climate and human evolution. *Science* 331, 540–542.

611 Dickinson, W.R., 1970. Interpreting detrital modes of graywacke and arkose. *J. Sediment. Petrol.* 40,
 612 695–707.

613 Dickinson, W.R., 1985. Interpreting provenance relations from detrital modes of sandstones, in:
 614 Zuffa, G.G. (Ed.), *Provenance of arenites*. Reidel Publ., Dordrecht, pp. 333–361.

615 Dott, R.H., 1964. Wacke, greywacke and matrix - what approach to immature sandstone
 616 classification? *J. Sediment. Petrol.* 34, 625–632.

617 Erlandson, J.M., 1994. *Early Hunter-Gatherers of the California Coast*, first ed. Plenum Press, New
 618 York.

619 Erlandson, J.M., 2001. The archaeology of aquatic adaptations: paradigms for a new millenium. *J.*
 620 *Archaeol. Res.* 9, 287–350.

621 Fernandes, M.E.B., 1991. Tool use and predation of oysters (*Crassostrea rhizophorae*) by the tufted
 622 capuchin, *Cebus apella apella*, in brackish water mangrove swamp. *Primates* 32, 529–531.
 623 Garzanti, E., 2016. From static to dynamic provenance analysis - Sedimentary petrology upgraded.
 624 *Sediment. Geol.* 336, 3–13.
 625 Gazzi, P., 1966. Le arenarie del flysch sopracretaceo dell' Appennino modenese: correlazioni con il
 626 flysch di Monghidoro. *Mineralogica et Petrographica Acta* 12, 69–97.
 627 Grantham, G.H., Marques, J.M., Wilson, M.G.C., Manhiça, V., Hartzer, F.J., 2011. Explanation of the
 628 Geological Map of Mozambique, 1:1,000,000. National Directorate of Geology, Maputo.
 629 GTK Consortium, 2006. Map Explanation – Sheets Central Mozambique, Vol. 2. National Directorate
 630 of Geology, Maputo.
 631 Harris, J.L., Leakey, M.G. (Eds.), 2003. Geology and Vertebrate Paleontology of the Early Pliocene Site
 632 of Kanapoi, Northern Kenya. *Contributions in Science* 498, Natural History Museum of Los
 633 Angeles County.
 634 Harrison, T., 2011. Hominins from the Upper Laetolil and Upper Ndolanya Beds, Laetoli, in: Harrison,
 635 T. (Ed.), *Paleontology and Geology of Laetoli: Human Evolution in Context*. Springer, Dordrecht,
 636 pp. 141–188.
 637 Hély, C., Bremond, L., Alleaume, S., Smith, B., Sykes, M.T., Guiot, J., 2006. Sensitivity of African
 638 biomes to changes in the precipitation regime. *Global Ecol. Biogeogr.* 15, 258–270.
 639 Hoffman, A., Pisera, A., Ryszkiewicz, M., 1974. Predation by muricid and naticid gastropods on the
 640 Lower Tortonian mollusks from the Korytnica clays. *Acta Geol. Pol.* 24, 249–264.
 641 Humle, T., Matsuzawa, T., 2009. Laterality in hand use across four tool-use behaviors among the wild
 642 chimpanzees of Bossou, Guinea, West Africa. *Am. J. Primatol.* 71, 40–48.
 643 Jarochovska, E., Tonarová, P., Munnecke, A., Ferrová, L., Sklenář, J., Vodrážková, S., 2013. An acid-
 644 free method of microfossil extraction from clay-rich lithologies using the surfactant Rewoquat.
 645 *Palaeontol. Electron.* 16, 1–16.

646 Joordens, J.C.A., 2011. The power of place: climate change as driver of hominin evolution and
647 dispersal over the past five million years. Ph.D. Dissertation, Vrije Universiteit Amsterdam.

648 Kaya, F., Bibi, F., Žliobaitė, I., Eronen, J.T., Hui, T., Fortelius, M., 2018. The rise and fall of the Old
649 World savannah fauna and the origins of the African savannah biome. *Nat. Ecol. Evol.* 2, 241–
650 246.

651 Kempf, E., 2009. Patterns of water use in primates. *Folia Primatol.* 80, 275–294.

652 Kilburn, R., Rippey, E. 1982. *Sea Shells of Southern Africa*, first ed. Macmillan, Johannesburg.

653 Kingdon, J., 2003. *Lowly Origin: Where, When, and Why our Ancestors First Stood Up*, first ed.
654 Princeton University Press, Princeton.

655 Lächelt, S., 2004. *The Geology and Mineral Resources of Mozambique*, first ed. National Directorate
656 of Geology, Maputo.

657 Luncz, L.V., Tan, A., Haslam, M., Kulik, L., Proffitt, T., Malaivijitnond, S., Gumert, M., 2017. Resource
658 depletion through primate stone technology. *eLife* 6, e23647.

659 Lutjeharms, J.R.E., 2006. *The Agulhas Current*, first ed. Springer, Berlin.

660 Lüdecke, T., Schrenk, F., Thiemeyer, H., Kullmer, O., Bromage, T.G., Sandrock, O., Fiebig, J., Mulch, A.,
661 2016a. Persistent C3 vegetation accompanied Plio-Pleistocene hominin evolution in the Malawi
662 Rift (Chiwondo BEDs, Malawi). *J. Hum. Evol.* 90, 163–175.

663 Lüdecke, T., Mulch, A., Kullmer, O., Sandrock, O., Thiemeyer, H., Fiebig, J., Schrenk, F., 2016b. Stable
664 isotope dietary reconstructions of herbivore enamel reveal heterogeneous savanna ecosystems
665 in the Plio-Pleistocene Malawi Rift. *Palaeogeogr. Palaeoclimatol. Palaeoecol.* 459, 170–181.

666 Macgregor, D., 2015. History of the development of the East African Rift System: A series of
667 interpreted maps through time. *J. Afr. Earth Sci.* 101, 232–252.

668 Malaivijitnond, S., Lekprayoon, C., Tandavanittj, N., Panha, S., Cheewatham, C., Hamada, Y., 2007.
669 Stone-tool usage by Thai long-tailed macaques (*Macaca fascicularis*). *Am. J. Primatol.* 69, 227–
670 233.

671 Mees, 2002. The nature of calcareous deposits along pan margins in eastern Central Namibia. *Earth*
672 *Surf. Proc. Land.* 27, 719–735.

673 Miall, A.D., 1996. *The Geology of Fluvial Deposits: Sedimentary Facies, Basin Analysis and Petroleum*
674 *Geology*, first ed. Springer, Berlin.

675 Müller, G., Gastner, M., 1971. The 'Karbonat-Bombe', a simple device for the determination of the
676 carbonate content in sediments, soils and other materials. *Neues Jahrb. Miner. Monatsh.* 10,
677 466–469.

678 Murphy, R.C., Kremer, J.N. 1992. Benthic community metabolism and the role of deposit-feeding
679 callianassid shrimp. *J. Mar. Res.* 50, 321–340.

680 Nicholson, S.E., 1996. A review of climate dynamics and variability in Eastern Africa, in: Johnson, T.C.,
681 Odado, E.O. (Eds), *The Limnology, Climatology and Paleoclimatology of the East African Lakes*.
682 Gordon and Breach, Amsterdam, pp. 22–56.

683 Partridge, T.C., 1997. Late Neogene uplift in eastern and southern Africa and its paleoclimatic
684 implications, in: Ruddiman, W.F. (Ed.), *Tectonic Uplift and Climatic Change*. Plenum Press, New
685 York, pp. 63–86.

686 Pettijohn, F. J., Potter, P. E., Siever, R., 1973. *Sand and Sandstone*, first ed. Springer, Berlin.

687 Phillips, W. J., 1965. The deformation of quartz in a granite. *Geol. J.* 4, 391–413.

688 Pickford, M., 2013. Gorongosa Palaeontology Survey. Report for Gorongosa National Park.

689 Pickford, M., Senut, B., 2001. The geological and faunal context of Late Miocene hominid remains
690 from Lukeino, Kenya. *Earth Planet. Sci.* 332, 145–152.

691 Plink-Björklund, P., 2005. Stacked fluvial and tide-dominated estuarine deposits in high-frequency
692 (fourth-order) sequences of the Eocene Central Basin, Spitsbergen. *Sedimentology* 52, 391–428.

693 Quade, J., Wynn, J.G. (Eds.), 2008. *The Geological Context of Human Evolution in the Horn of Africa*.
694 *Geol. Soc. Am. Spec. Publ.* 446, Boulder.

695 Real, F., 1966. Geologia da bacia do rio Zambeze (Moçambique): características geológico-mineiras
696 da bacia do rio Zambeze, em território Moçambicano. Junta de Investigações do Ultramar,
697 Lisboa.

698 Ryan, W.B.F., Carbotte, S.M., Coplan, J.O., O'Hara, S., Melkonian, A., Arko, R., Weissel, R.A., Ferrini,
699 V., Goodwillie, A., Nitsche, F., Bonczkowski, J., Zemsky, R., 2009. Global Multi-Resolution
700 Topography synthesis. *Geochem. Geophys. Geosy.* 10, Q03014.

701 Salman, G., Abdula, I., 1995. Development of the Mozambique and Ruvuma sedimentary basins,
702 offshore Mozambique. *Sediment. Geol.* 96, 7–41.

703 Schlüter, P., Uenzelmann-Neben, G., 2007. Seismostratigraphic analysis of the Transkei Basin: a
704 history of deep sea current controlled sedimentation. *Mar. Geol.* 240, 99–111.

705 Schrenk, F., Bromage, T.G.; Betzler, C.G., Ring, U., Juwayeyi, Y.M., 1993. Oldest Homo and Pliocene
706 biogeography of the Malawi Rift. *Nature* 365, 833–836.

707 Ségalen, L., Lee-Thorp, J., Cerling, T., 2007. Timing of C4 grass expansion across sub-Saharan Africa. *J.*
708 *Hum. Evol.* 53, 549–559.

709 Spötl, C., Vennemann, T.W., 2003. Continuous-flow isotope ratio mass spectrometric analysis of
710 carbonate minerals. *Rapid Commun. Mass Spectrom.* 17, 1004–1006.

711 Steinbruch, F., 2010. Geology and geomorphology of the Urema Graben with emphasis on the
712 evolution of Lake Urema. *J. Afr. Earth Sci.* 58, 272–284.

713 Tinley, K.L., 1977. Framework of the Gorongosa ecosystem Mozambique. Ph.D. Dissertation,
714 University of Pretoria.

715 Uenzelmann-Neben, G., Schlüter, P., Weigelt, E., 2007. Cenozoic ocean circulation within the South
716 African gateway: indications from seismic stratigraphy. *S. Afr. J. Geol.* 110, 275–294.

717 White, T.D., Ambrose, S.H., Suwa, G., Su, D.F., DeGusta, D., Bernor, R.L., Boisserie, J.R., Brunet, M.,
718 Delson, E., Frost, S., Garcia, N., Giaourtsakis, I.X., Haile-Selassie, Y., Howell, F.C., Lehmann, T.,
719 Likius, A., Pehlevan, C., Saegusa, H., Semprebon, G., Teaford, M., Vrba, E., 2009.

Macrovertebrate paleontology and the Pliocene habitat of *Ardipithecus ramidus*. *Science* 326, 87–93.

Wieder, M., Yaalon, D.H., 1982. Micromorphological fabrics and developmental stages of carbonate nodular forms related to soil characteristics. *Geoderma* 28, 203–220.

Wrangham, R.W. 2005. The delta hypothesis: hominoid ecology and hominin origins, in: Lieberman, D.E., Smith, R.J., Kelley, J. (Eds.), *Interpreting the Past: Essays on Human, Primate and Mammal Evolution in Honor of David Pilbeam*. Brill Academic Publishers, Boston, pp. 231–242.

Zaitlin, B.A., Dalrymple, R.W., Boyd, R., 1994. The stratigraphic organization of incised-valley systems associated with relative sea-level changes, in: Dalrymple, R.W., Boyd, R., Zaitlin, B.A. (Eds.), *Incised-Valley Systems: Origin and Sedimentary Sequences*. SEPM Spec. Publ. 51, pp. 45–60.

Figure captions

Table 1. Petrographic data (mineralogical and modal compositions in vol.%) obtained from thin-sectioned sedimentary rock samples by the Gazzi-Dickinson point-counting method (Gazzi, 1966; Dickinson, 1970). See also Appendix A.

Table 2. Paleocurrent directions reconstructed from measurements of directional transport indicators. See also Appendix B.

Fig. 1. Geographic overview. (A) Topographic map and (B) cross-section showing the position of GNP in central Mozambique. The map was generated with GeoMapApp (<http://www.geomapapp.org>, accessed September 2016) using the Global Multi-Resolution Topography basemap of Ryan et al. (2009). Map inset displays the position of the East African Rift System (black) and the major air boundaries over Africa in January (yellow) and July (purple): ITCZ = Intertropical Convergence Zone, CAB = Congo Air Boundary (Nicholson, 1996).

Sea-surface circulation during February (North East Monsoon season) is illustrated for the Indian Ocean (Lutjeharms, 2006).

Fig. 2. Geological framework and study areas. (A) Geological map of GNP and its surroundings, (B) vertical geological cross-section of the Urema Rift stretching from Mount Gorongosa to Inhaminga village (modified from Lächelt, 2004), and (C) detailed map section showing the position of the study sites (GPL = Gorongosa Paleontological Locality). We herein use ‘Mazamba Formation’ to collectively refer to this ~130 m thick succession (Lächelt, 2004; Steinbruch, 2010) and differentiate a lower and an upper (Inhaminga) member (Real, 1966; Tinley, 1977; Pickford, 2013).

Fig. 3. Correlated stratigraphic sections measured at GPL-1SW, GPL-1NE, GPL-8, GPL-6, GPL-9, and GPL-2. The studied succession from the lower member of the Mazamba Formation is interpreted as a coastal-plain estuarine record that formed prior to rifting as compound incised valley-fill in a shallow-ramp setting following transgression. See Fig. 2C for location of measured sections.

Fig. 4. Bulk sediment petrography (Table 1, Appendix A) and paleocurrent directions (Table 2, Appendix B). (A) Petrographic classification of granule conglomerates, sandstones, and wackes based on QFL (quartz-feldspar-lithics) data normalized to 100 %. Nomenclature scheme after Garzanti (2016), following Crook (1960) and Dickinson (1970). (B) Petrographic data and provenance inferences (CB = continental block, MA = magmatic arc, RO = recycled orogenic) with subdivisions based on Dickinson (1985) and reference data from Garzanti (2016). (C) Mineralogical and modal composition of granule conglomerates, sandstones, wackes, and sandy clay- and marlstones, based on major component data normalized to 100 % (see Fig. 3

for position of samples within measured stratigraphic sections). (D) Rose diagram illustrating paleocurrent directions (corrected for -11° local declination) reconstructed from measurements of directional transport indicators (Table 2, Appendix B).

Fig. 5. Thin-section photomicrographs illustrating detrital characteristics and invertebrate fossil contents of selected rock samples. (A-F) Overview photomicrographs (plane-polarized light) of samples related mainly to the GPL-1SW section: (A) sample GPL9-01, Facies 2, sparry calcite-cemented fluvial granule conglomerate; (B) sample GPL1SW-01, Facies 2, sparry calcite-cemented granule-bearing fluvial sandstone; (C) sample GPL1SW-02, Facies 3, fluvial bay-head delta wacke; (D) sample GPL1SW-05, Facies 5, transitional bay-head delta/estuarine central basin wacke; (E) sample GPL1SW-06, Facies 6, estuarine central basin sand-bearing marly claystone; (F) sample 16-Gor-Muar-1, sparry calcite-cemented littoral(?) sandstone. (G-L) Details of sample GPL1-01 (A) as seen in cross-polarized light: (G) overview photomicrograph displaying spar-cemented, loosely-packed mono- and poly-quartz grains; (H, I) plutoniclastic granite rock fragments consisting of quartz and feldspar (H) and quartz (I), respectively, with coarse interlocking mosaic of crystals; (J) detail of eogenetic drusy mosaic-textured sparry calcite cement (note also spar-filled cast of dissolved bioclastic fragment in the lower part of the image); (K) skeletal grain of a corallinacean red algae (note fine net-like, multi-layered internal structure); (L) bioclastic wall fragment of a serpulid worm tube consisting of two microstructurally different layers. (M-O) Details of sample 16-Gor-J02 (C) as seen in plane- and cross-polarized light, showing detrital matrix consisting of clay (M, N) or silty clay (O). See Fig. 2 for position of samples within measured stratigraphic sections.

Fig. 6. Selected specimens of fossil vertebrates from GPL-1. (A) *In situ* mammalian rib immediately after excavation (sample PPG2016-P-18), (B) proboscidean metacarpal bone (sample PPG2017-

P-122c), (C) shark tooth fragment (sample PPG2017-P-121b), (D) suid upper incisor (sample PPG2017-P-75-1). Specimens (A-C) were found *in situ*, deriving respectively from the lower, middle, and upper fossiliferous level in the GPL-1NE section (Fig. 3); specimen (D) is a surface find from GPL-1. See Fig. 2C for location of GPL-1 and Fig. 3 for measured stratigraphic sections.

Fig. 7. Invertebrate fossils from the fossiliferous sandstone of Facies 11 at GPL-2. (1, 2) Left propodus of a member of the family Callianassidae; inner (1) and outer (2) view. (3, 4) Two disarticulated left dactyli of decapod crustaceans. (5-7) *?Terebralia palustris*; apical (5), and lateral (6, 7) views. (8-12) Shells of members of the family Cerithiidae; lateral views. (13) *Rhinoclavis* sp., lateral view. (14, 15) *?Striostrea* sp.; left valve. (16-27) *Striostrea margaritacea*; right (16-18, 21-27) and left (19, 20) valves. Note the common traces of barnacle attachments on the shells (e.g., 23-25) and the boring attributable to a muricid gastropod (25-27). Scale bar: 10 mm (1-13), 15 mm (14-26), 4 mm (27). See Fig. 2C for location of GPL-2 and Fig. 3 for measured stratigraphic section.

Fig. 8. Selected specimens of fossil wood from Menguere Hill. (A, B) Basal stump of a large palm tree (A) with the numerous roots, broken naturally to show the vascular strands in the root sheaths (B). (C, D) Outer surface (C) and cross section (D) of large trunks of dicot wood with diameters >1 m. (E, F) Photomicrographs of sample BP-16-1731 (*Terminalioxylon* sp.) taken from trunk cross section shown in (D). (E) Transverse section displaying large vessels (average tangential diameter is 285 µm) arranged in short radial multiples of 1-3 cells, and lighter cells partially surrounding them that represent the parenchyma cells (vasicentric to aliform). Ground tissue is composed of fibres. (F) Tangential longitudinal section showing uniseriate rays with long narrow fibres in between. (G) Rays with procumbent body cells and square marginal cells as

seen in radial longitudinal section. Parenchyma is vasicentric to aliform, even sometimes unilateral and the strands are 2 cells long. See Fig. 2C for location of Menguere Hill.

Fig. 9. Miocene pre-rift paleogeographic reconstruction. The block model illustrates depositional environments and coastal ecosystem mosaics reconstructed for the lower member of the Mazamba Formation. The studied succession records a transgressive trend from continental lowstand (fluvial, alluvial) to transgressive and highstand conditions (estuarine, marine). Estuarine and lagoonal organizational features redrawn from Boyd et al. (2006). See Fig. 2 for stratigraphy (key to colors and abbreviations).

Appendix A. Petrographic data (mineralogical and modal compositions in vol.%) obtained from thin-sectioned sedimentary rock samples by the Gazzi-Dickinson point-counting method (Gazzi, 1966; Dickinson, 1970). See also Table 1.

Appendix B. Paleocurrent directions reconstructed from measurements of directional transport indicators. See also Table 2.

Appendix C. Stable isotope data of pedogenic carbonates and calibration standards.

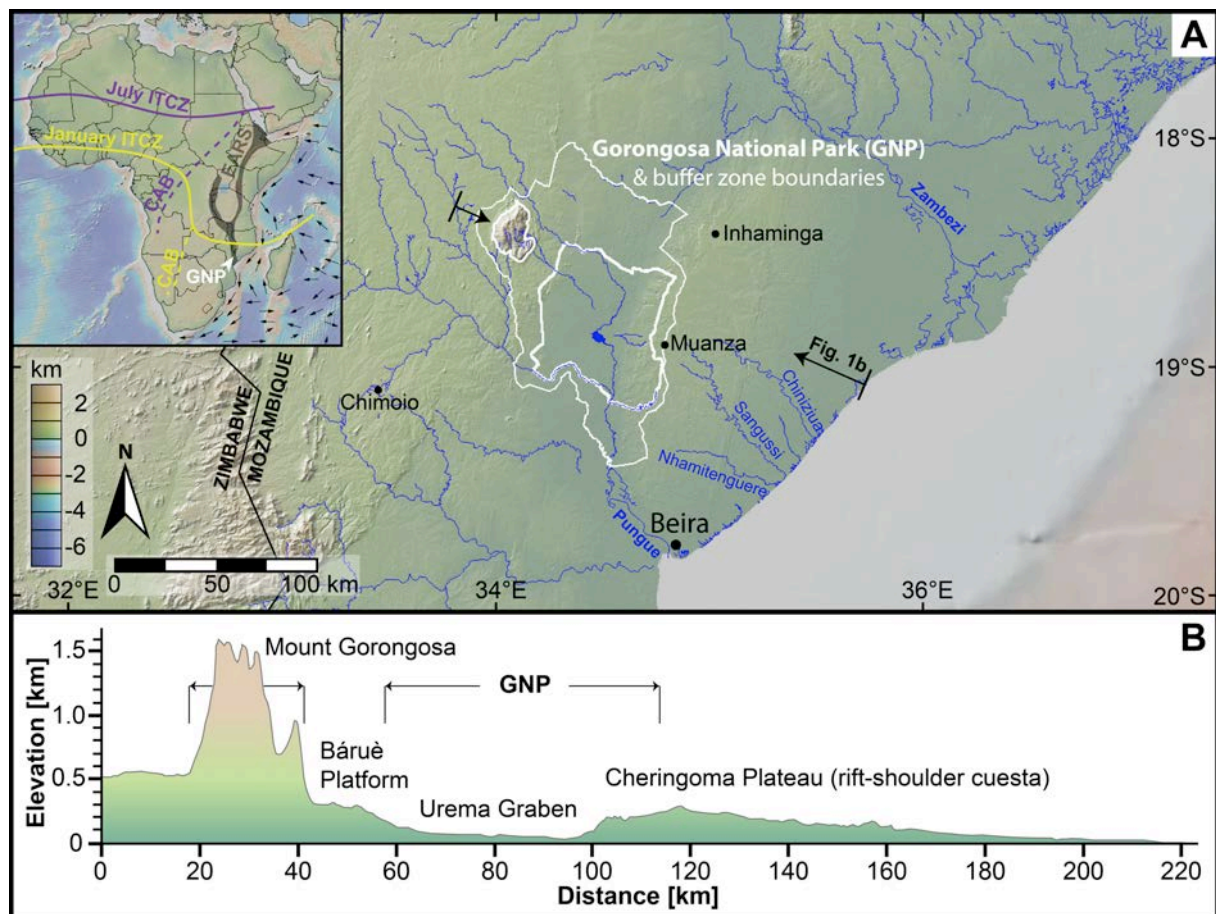


Fig. 1

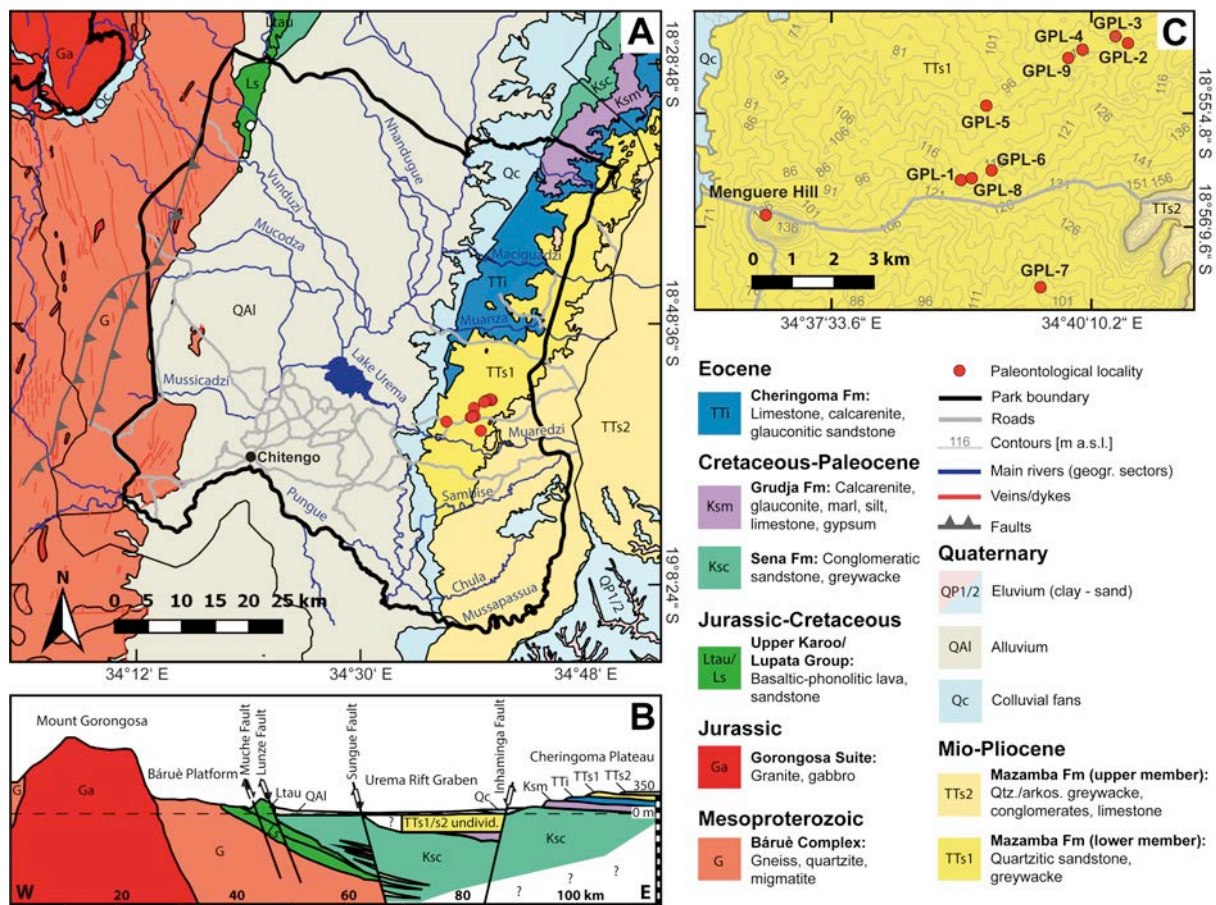


Fig. 2

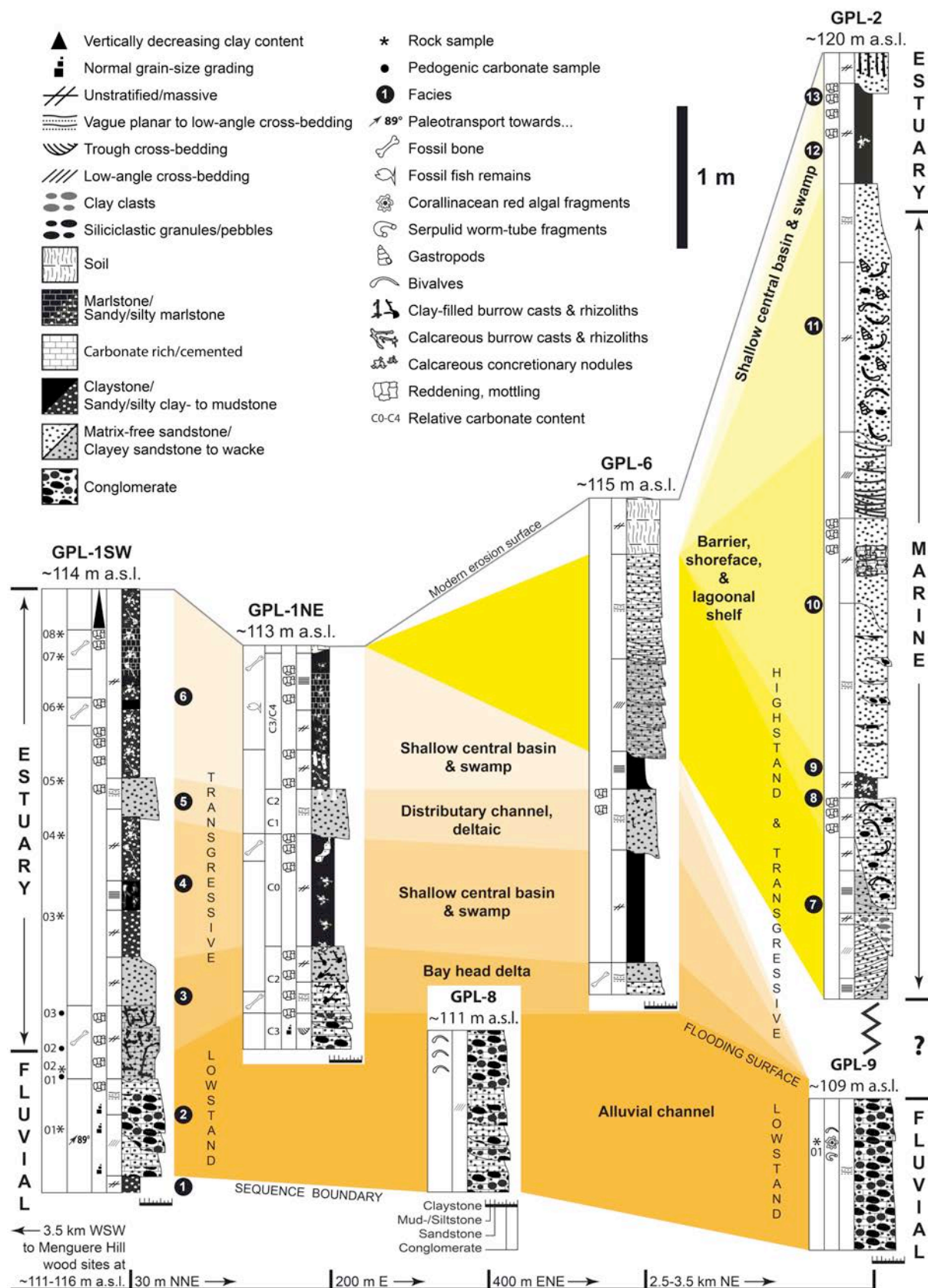


Fig. 3

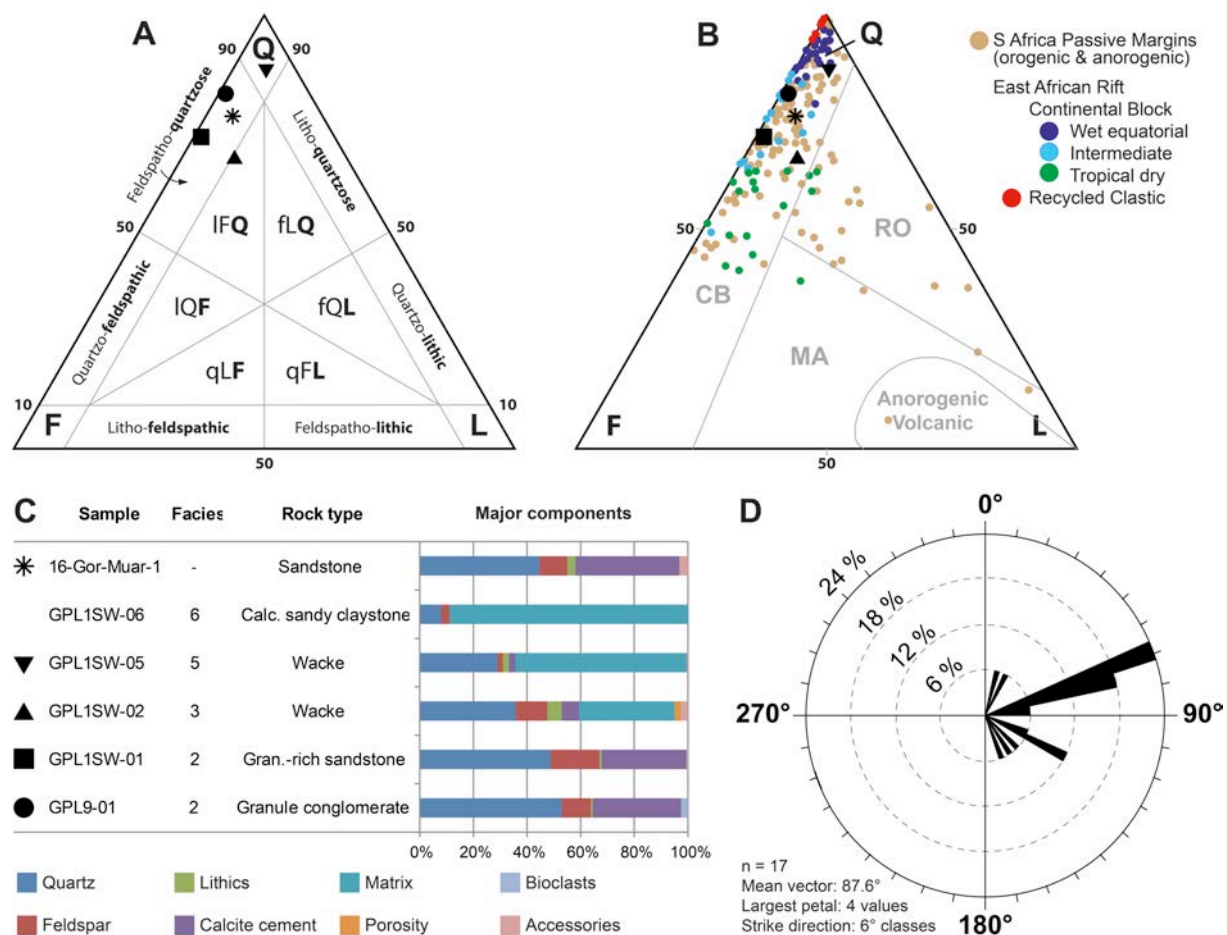


Fig. 4

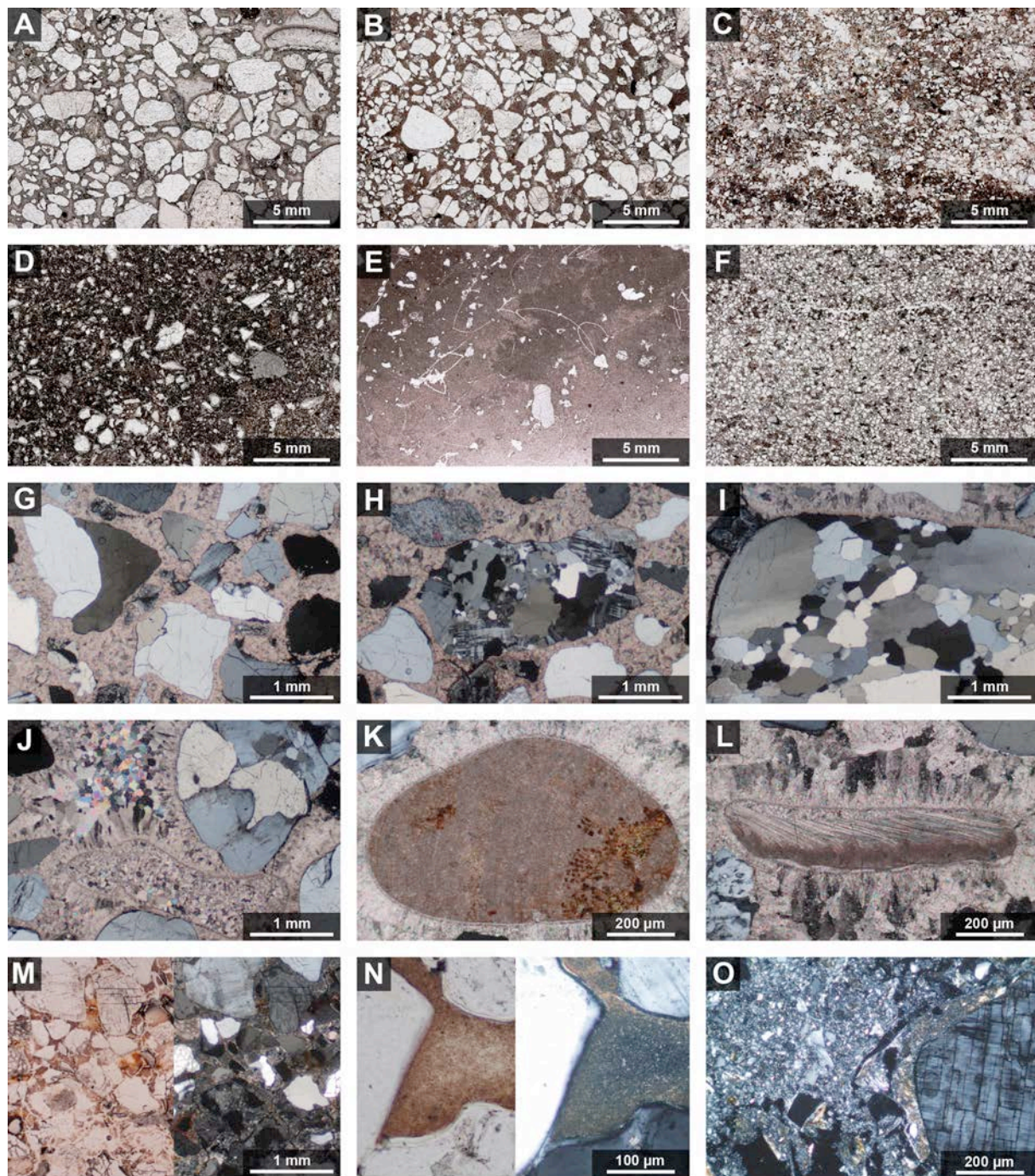


Fig. 5

857
858
859
860
861

862

863

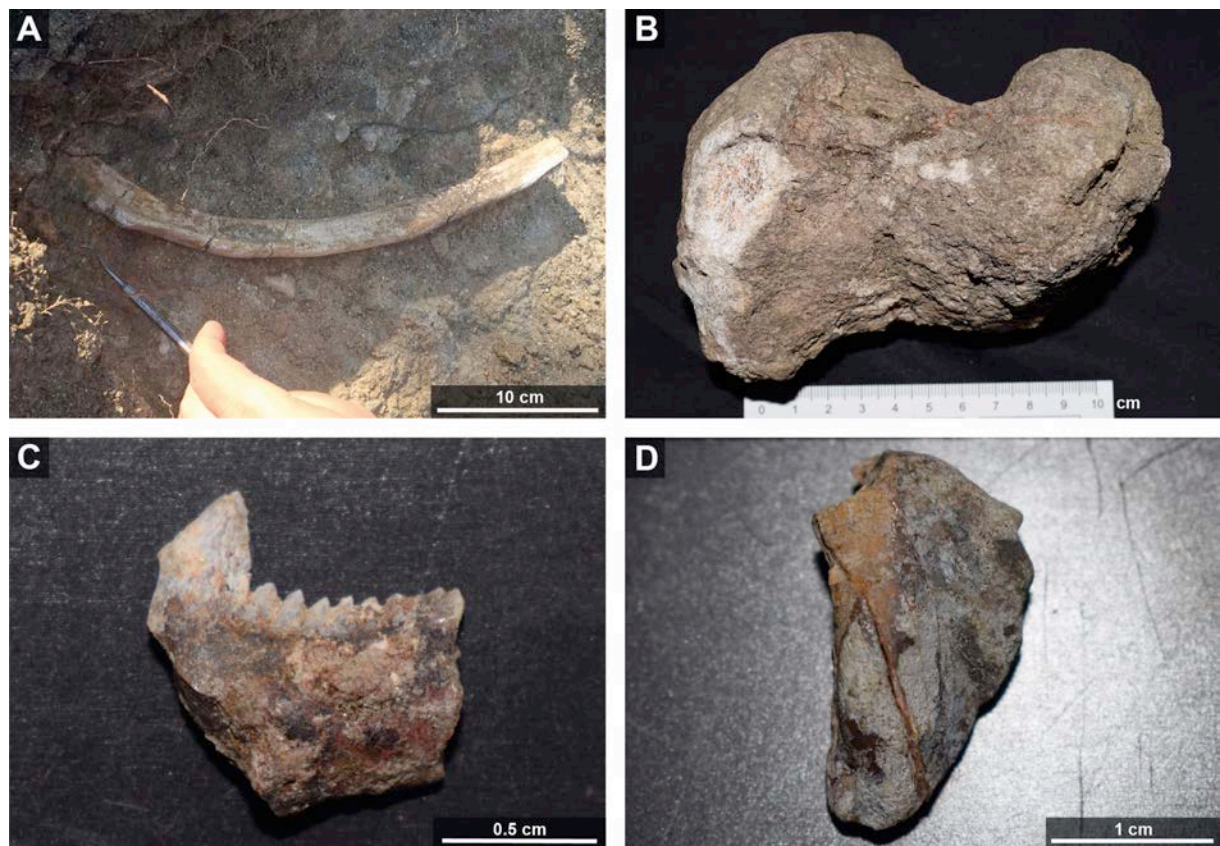


Fig. 6

864

865

866

867

868

869

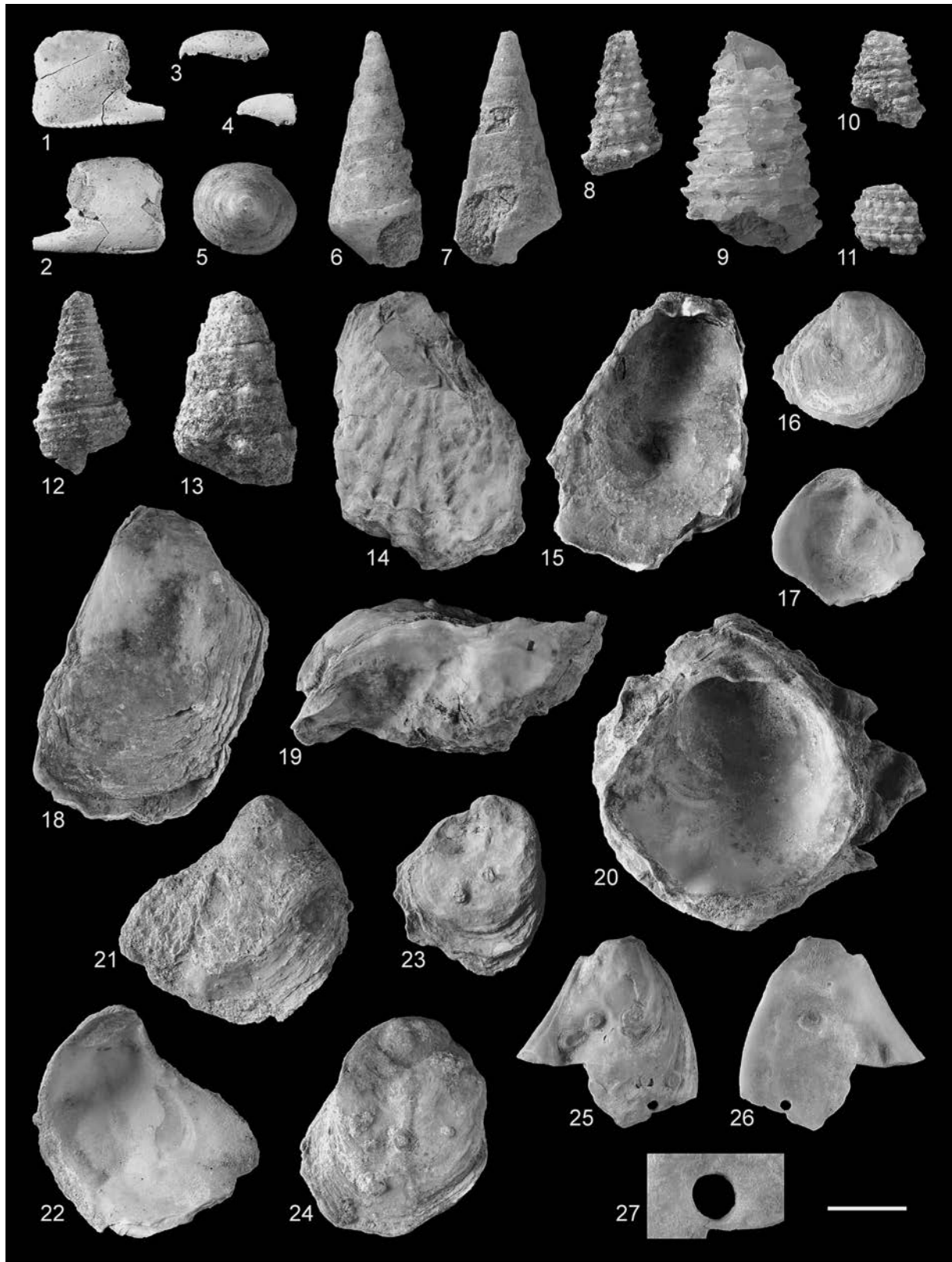


Fig. 7

870

871

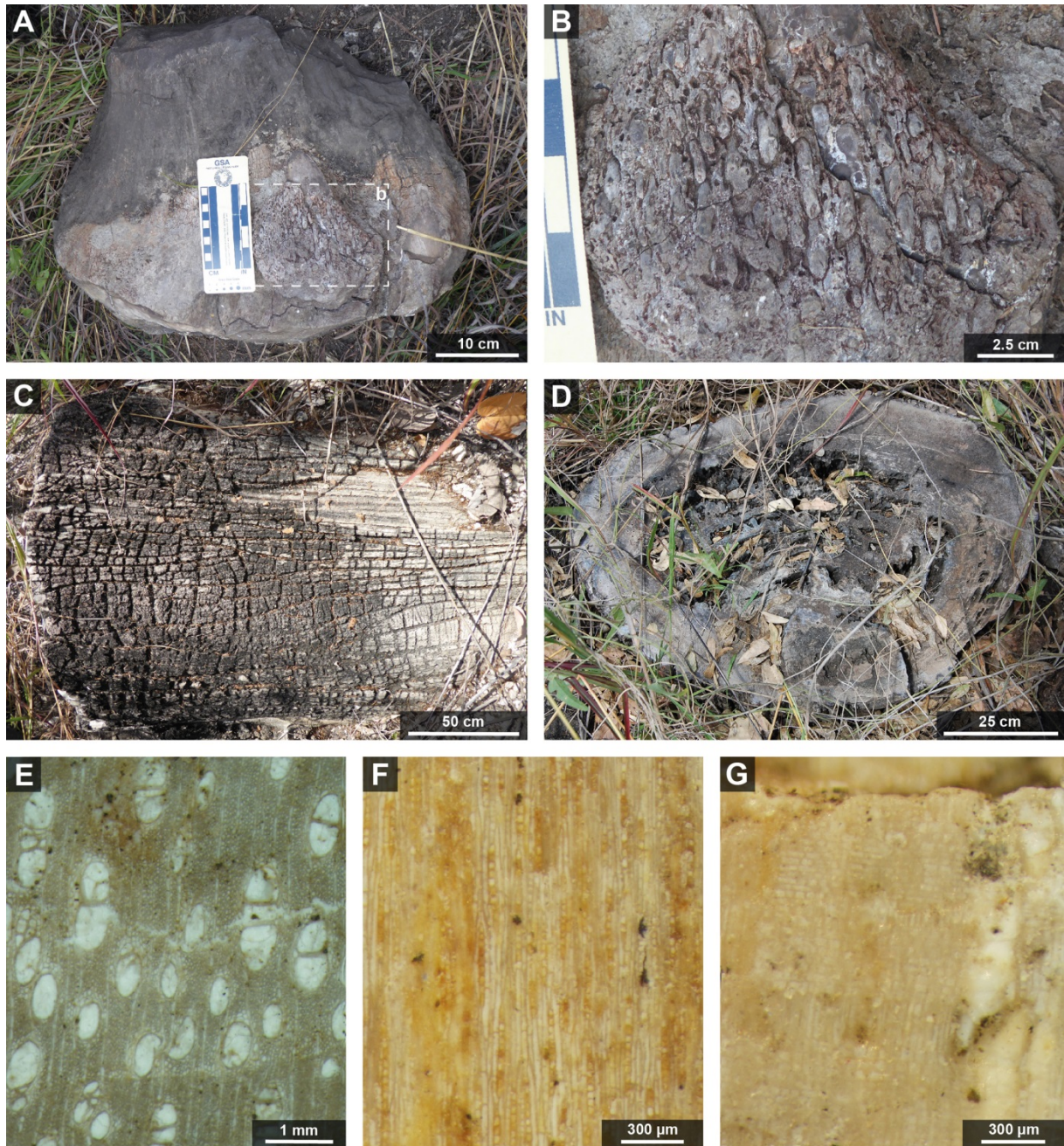
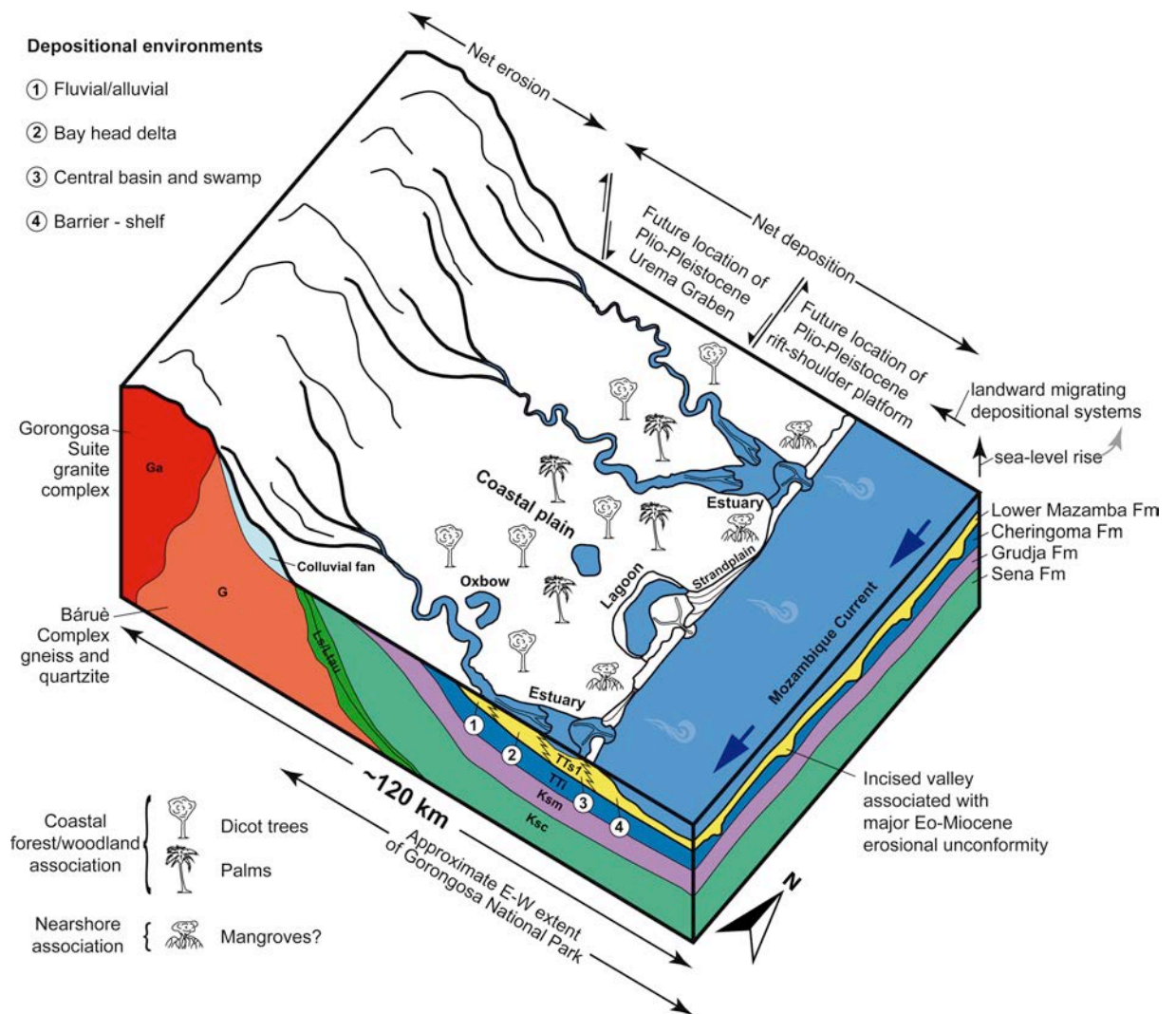


Fig. 8

872



Sample	Facies	Grain size	Quartz			Feldspar (K-fsp + plag)		Micas		Heavy miner.	Lithics			Bioclasts	Cement		Matrix	Void	CaCO ₃ *	Rock type
			Monocr.	Monocr., str.	In pluton., str.	Monocr.	In pluton.	Biotite	Muscovite		Chert	Clayclast	Dolerite		Sparry calcite	Phyllosilicate	Silicate	Pore		
16-Gor-Muar-1	-	mS	3.5	35.8	6.8	10.3	0.2	1.8	-	0.2	-	1.8	0.2	-	39.2	-	-	-	n.d.	Sandstone
GPL1SW-08	6	C-mS	n.d.	n.d.	n.d.	n.d.	n.d.	n.d.	n.d.	n.d.	n.d.	n.d.	n.d.	n.d.	n.d.	n.d.	n.d.	n.d.	39.5	Sandy marlstone
GPL1SW-07	6	C-mS	n.d.	n.d.	n.d.	n.d.	n.d.	n.d.	n.d.	n.d.	n.d.	n.d.	n.d.	n.d.	n.d.	n.d.	n.d.	n.d.	25.0	Calc. sandy claystone
GPL1SW-06	6	C-mS	0.2	7.8	-	3.0	-	-	-	-	-	-	-	-	-	-	88.8	-	25.0	Calc. sandy claystone
GPL1SW-05	5	C-cS	-	28.0	1.0	1.8	0.2	-	-	0.2	-	-	-	-	4.7	-	63.8	0.2	n.d.	Wacke
GPL1SW-02	3	C-cS	1.6	32.2	2.0	11.0	0.8	0.2	0.2	1.9	-	-	0.6	0.2	11.3	-	35.6	2.5	n.d.	Wacke
GPL1SW-01	2	cS-gr.	10.0	32.5	6.2	16.2	2.0	0.2	-	0.2	-	-	0.8	0.2	31.5	-	-	-	n.d.	Gr.-rich sandstone
GPL9-01	2	cS-gr.	1.0	39.8	12.2	10.8	-	-	-	-	-	0.5	0.2	2.5	33.0	-	-	-	n.d.	Gr. conglom.

Abbreviations: C = clay, mS = medium sand, cS = coarse sand, gran. = granule conglomerate, Monocr. = monocrystal, In pluton. = in plutonic rock fragment, str. = strained, Biot. = biotite, Musc. = muscovite, Claycl. = clayclasts, Biocl. = bioclasts, n.d. = not determined, - = not detected. 400 grains were counted per sample. *CaCO3 contents were determined by whole-rock analysis using the “Karbonat-Bombe” technique (Müller and Gastner, 1971). See Fig. 3 for position of samples within measured stratigraphic sections and Fig. 4A-C for data plots.

Sector	Coordinates		Stratigraphy	Transport indicator	Strike/dip direction	Paleocurrent towards*	
	Latitude	Longitude				uncorrected	corrected
Mussapassua	-19.093538	34.720811	Mazamba upper	imbrication	204°/28°	24°	13°
Mussapassua	-19.093538	34.720811	Mazamba upper	imbrication	260°/30°	80°	69°
Muaredzi	-18.928747	34.647454	Mazamba lower	channel	100°-280°	100°	89°
Muaredzi	-18.928747	34.647454	Mazamba lower	bone long axis	85°-165°	85°	74°
Muaredzi	-18.928747	34.647454	Mazamba lower	bone long axis	120°-300°	120°	109°
Muaredzi	-18.914741	34.666622	Mazamba lower	channel	40°-220°	40°	29°
Muaredzi	-18.914741	34.666622	Mazamba lower	imbrication	265°/30°	85°	74°
Muaredzi	-18.914741	34.666622	Mazamba lower	foreset	90°/25°	90°	79°
Muaredzi	-18.914741	34.666622	Mazamba lower	trough	80°-260°	80°	69°
Muaredzi	-18.912068	34.672796	Mazamba lower	trough	80°-260°	80°	69°
Muaredzi	-18.912550	34.668370	Mazamba lower	channel	80°-260°	80°	69°
Muaredzi	-18.906120	34.673520	Mazamba lower	channel	85°-260°	85°	74°
Muaredzi	-18.849300	34.662800	Mazamba lower	imbrication	335°/15°	155°	144°
Muaredzi	-18.849300	34.662800	Mazamba lower	imbrication	310°/25°	130°	119°
Muaredzi	-18.849300	34.662800	Mazamba lower	imbrication	325°/20°	145°	134°
Muaredzi	-18.849300	34.662800	Mazamba lower	imbrication	350°/30°	170°	159°
Muaredzi	-18.902500	34.671900	Mazamba lower	channel	130°-310°	130°	119°

*Uncorrected/corrected for -11° local declination (August 2016). See Fig. 1 for location of geographic sectors and Fig. 4D for rose diagram. Although channel- and trough-axes are bipolar paleocurrent indicators, a unipolar direction is deduced based on consideration of the broader geomorphological context (i.e., topographic highs west of the Urema Graben) and provenance data.

894

895

896

897

898